nature chemical biology

ARTICLES

https://doi.org/10.1038/s41589-018-0195-0

A chemical–genetic screen identifies ABHD12 as an oxidized-phosphatidylserine lipase

Dhanashree S. Kelkar[1,3], Govindan Ravikumar[2,3], Neelay Mehendale[1,3], Shubham Singh[1,3], Alaumy Joshi[1], Ajay Kumar Sharma[2], Amol Mhetre[1], Abinaya Rajendran[1], Harinath Chakrapani[2] and Siddhesh S. Kamat[1*]

Reactive oxygen species (ROS) are transient, highly reactive intermediates or byproducts produced during oxygen metabolism. However, when innate mechanisms are unable to cope with sequestration of surplus ROS, oxidative stress results, in which excess ROS damage biomolecules. Oxidized phosphatidylserine (PS), a proapoptotic 'eat me' signal, is produced in response to elevated ROS, yet little is known regarding its chemical composition and metabolism. Here, we report a small molecule that generates ROS in different mammalian cells. We used this molecule to detect, characterize and study oxidized PS in mammalian cells. We developed a chemical–genetic screen to identify enzymes that regulate oxidized PS in mammalian cells and found that the lipase ABHD12 hydrolyzes oxidized PS. We validated these findings in different physiological settings including primary peritoneal macrophages and brains from *Abhd12*$^{-/-}$ mice under inflammatory stress, and in the process, we functionally annotated an enzyme regulating oxidized PS in vivo.

Oxidative stress is an imbalance between cellular oxidants and antioxidants in favor of oxidants, which leads to the disruption of redox signaling and has been implicated in several human pathophysiologies[1–4]. Under oxidative stress, excess ROS, namely superoxide, hydrogen peroxide (H_2O_2) and hydroxyl radicals, cannot be detoxified through innate coping mechanisms[5], and consequently damage cellular components and cause cell death via apoptosis or necrosis[5]. Lipid membranes serve as cells' first line of defense against ROS by providing a physical barrier to ROS diffusion; therefore, membranes are primary targets for oxidative damage[5]. When ROS are generated near cellular membranes, the constituent lipids, particularly those bearing polyunsaturated fatty acid (PUFA) chains, are oxidized[6,7]. The resulting oxidized lipids disrupt the local membrane structure and integrity, and thus impair cellular functions by modulating the activity of a wide array of important cellular proteins[8,9]. Previously, research groups have focused on the oxidation of a single PUFA[6,7], but little is known regarding the global lipid profile under oxidative stress[8,9] and the enzymatic pathways that metabolize those oxidized lipid products in vivo.

PS, a phospholipid localized to the inner-membrane leaflet, has several critical functions in mammalian biology[10]. Important among these is its role in ROS signaling and apoptosis[11]. Given the asymmetric distribution of PS in the membrane bilayer, the externalization of PS reflects a stressed cell, and this 'flipped' PS is recognized by phagocytes as an 'eat me' signal[12–14]. Several studies have suggested that under oxidative stress, surplus ROS reacts with the *sn*-2-esterified PUFAs of PS, thus producing oxidized PS[6], which has a flipped membrane orientation; the oxidized PS then acts as an apoptotic signal[12,14]. Although these studies have described the production and role of oxidized PS in apoptosis, little is known regarding its metabolism. Physiologically, this metabolism is important, because several cells require high oxygen tension (for example, neurons, macrophages and cancer cells) and consequently have elevated ROS, which produce oxidized PS in a constant flux. However, innate mechanisms within such cells can efficiently metabolize oxidized PS and prevent apoptosis.

In this paper, we synthesized and characterized a small molecule that generates ROS efficiently in mammalian cells and developed mass spectrometry methods to study oxidized PS; using both in tandem, we performed a chemical–genetic screen to identify lipases capable of metabolizing oxidized PS. We found that the serine hydrolase (SH) enzyme ABHD12 (α/β hydrolase domain (ABHD) protein 12) is a major oxidized-PS lipase. We validated these findings through complementary biochemical, pharmacological and genetic assays in different physiological systems. Importantly, we found that ABHD12 controls levels of oxidized PS in the mammalian brain under severe inflammatory stress. Given the central role of ABHD12 in the human neurological disease polyneuropathy, hearing loss, ataxia, retinitis pigmentosa and cataract (PHARC)[15,16], its role in metabolizing oxidized PS adds another avenue toward understanding the PHARC pathophysiology.

Results

Characterization of an esterase-activated ROS probe. 1,4-Dihydroquinones react with oxygen, thereby generating superoxide, which spontaneously dismutates to hydrogen peroxide[17,18]. Among these compounds, the 'juglones' have been found to be effective against several antibiotic-resistant bacteria[19]. Nonetheless, very few probes of this scaffold are used to study ROS signaling in mammalian cells. The lack of intramolecular hydrogen bonding makes these molecules poor ROS generators;[17,18] hence, installing a metabolically cleavable linker that after activation restores this ability provides opportunities to trigger ROS generation on demand in mammalian cells. With this rationale, we synthesized MGR1 (**1**), 5-hydroxy-1,4,4a,9a-tetrahydro-1,4-ethanoanthracene-9,10-dione

[1]Department of Biology, Indian Institute of Science Education and Research (IISER), Pune, India. [2]Department of Chemistry, Indian Institute of Science Education and Research (IISER), Pune, India. [3]These authors contributed equally: Dhanashree S. Kelkar, Govindan Ravikumar, Neelay Mehendale, Shubham Singh. *e-mail: siddhesh@iiserpune.ac.in

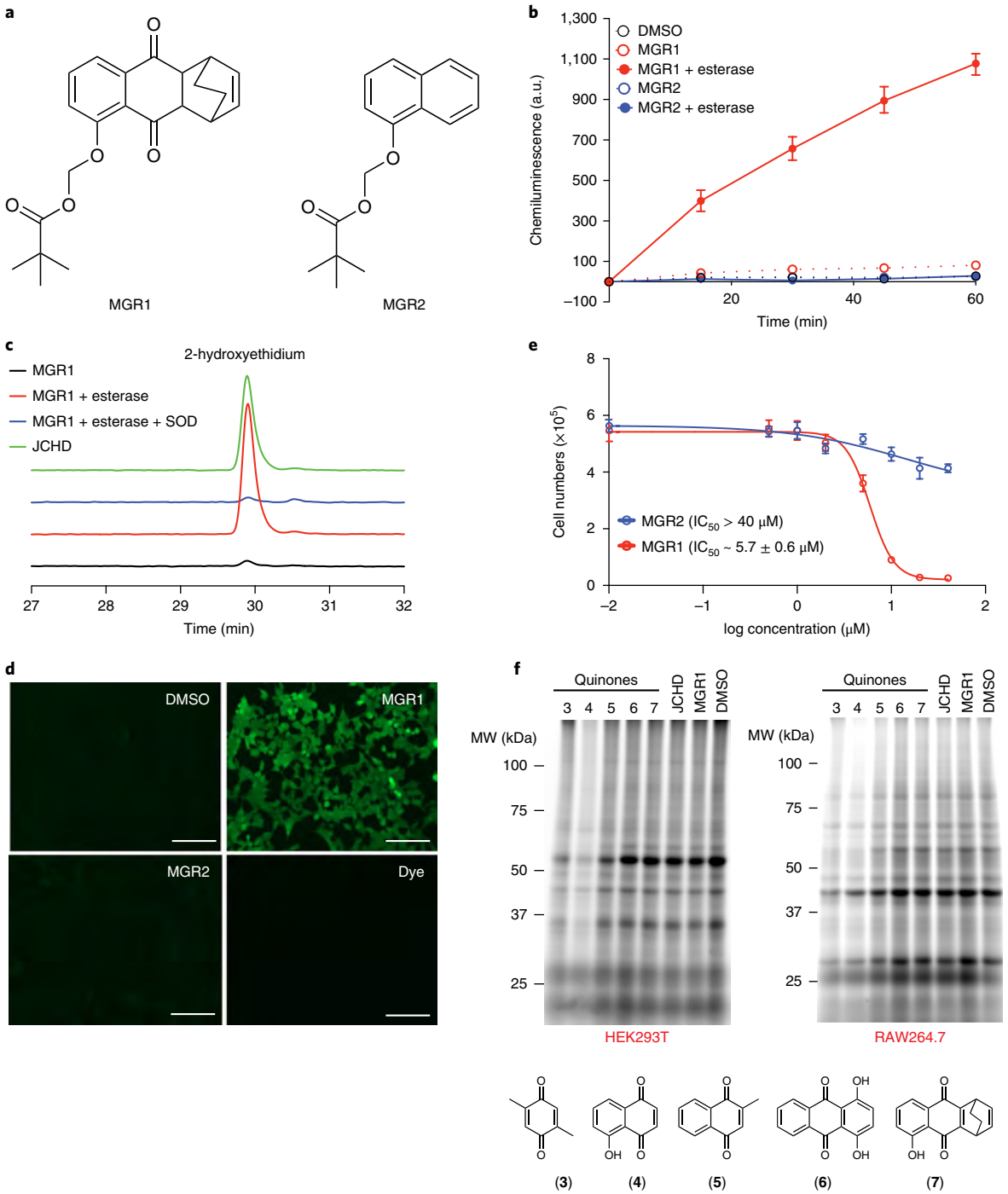

Fig. 1 | Characterization of a ROS-generating probe (MGR1), and an inactive control probe (MGR2). a, Chemical structures of the active dihydroquinone ROS generator MGR1 (**1**) and the inactive 1-naphthol control compound MGR2 (**2**). **b**, Luminol-based chemiluminescence assay showing robust in vitro superoxide production by MGR1 but not MGR2, in the presence of esterase. The assay was performed at 37 °C, and each time point represents the mean ± s.e.m. in arbitrary units (a.u.) of chemiluminescence intensity from three independent experiments. **c**, HPLC traces showing the robust formation of superoxide (2-hydroxyethidium formation from hydroethidine) from MGR1 in the presence of esterase. This superoxide production from MGR1 in the presence of an esterase was ablated by SOD. JCHD was used as a positive control in this experiment. This experiment was performed in triplicate and yielded reproducible results. **d**, Chemifluorescence showing the robust cellular production of ROS by MGR1, but not MGR2, in HEK293T cells treated with MGR1 or MGR2 (25 μM, 1 h), and subsequently chased with 10 μM DCF for 10 min. Scale bars, 200 μm. The assay was performed per the manufacturer's instructions as three independent experiments yielding reproducible results. Additional information can be found in Supplementary Fig. 5. **e**, Cell viability assays showing cell death of HEK293T cells under higher concentrations of MGR1 (>5 μM), but not MGR2, owing to heightened ROS production. Data are shown as mean ± s.e.m. for 4 independent replicates, and the 95% confidence interval for the reported IC_{50} value of MGR1 is 5.1–6.3 μM. **f**, Gel-based chemoproteomics showing negligible proteome-wide thiol reactivity of MGR1 treated with esterase compared with other reactive quinones (3–7) in HEK293T and RAW264.7 cell lysates. All compounds were used at 100 μM for 1 h and subsequently chased with 1 mM IAA (1 h), after which click reaction was performed. MW, molecular weight. This experiment was performed in triplicate and yielded reproducible results.

(JCHD)[17], with an esterase-activated handle (Fig. 1a). We postulated that MGR1 would be activated by the ubiquitous esterases[20] in mammalian cells and produce ROS (Supplementary Fig. 1). To control for any structural effects of MGR1, we also synthesized a structural analog, MGR2 (**2**), which has a naphthalene moiety and is unable to produce ROS (Fig. 1a). To validate the ROS-production abilities of MGR1 and MGR2, we first performed a chemiluminescence assay[21] and found that MGR1 but not MGR2 robustly produced ROS only when acted upon by an esterase (Fig. 1b). In agreement with the proposed mechanism (Supplementary Fig. 1), we found that pretreatment or incubation with a broad-spectrum SH inhibitor (fluorophosphonate (FP)-alkyne)[20] or superoxide dismutase (SOD), respectively, ablated the ROS-generating ability of MGR1 in vitro (Supplementary Fig. 2). Next, we detected 2-hydroxyethidium (2-HE) from hydroethidine, owing to superoxide from MGR1 only in the presence of esterase, by high-performance liquid chromatography (HPLC)[22] (Fig. 1c). SOD prevented 2-HE formation from MGR1 in the presence of an esterase, in agreement with superoxide formation from MGR1 after esterase activation (Fig. 1c). We also confirmed by HPLC analysis, that after esterase activity, MGR1 and MGR2 produced JCHD and 1-naphthol, respectively (Supplementary Fig. 3).

Next, we compared the ROS-producing capability of MGR1 with those of MGR2, xenobiotics (menadione, artemisinin, cisplatin and paraquat) and ROS generators (JCHD, oxidized JCHD and H_2O_2), by using luminol-based chemiluminescence assays (Supplementary Fig. 2) and a commercial 2′,7′-dichlorodihydro-fluorescein diacetate (DCF) cellular ROS-detection assay (Supplementary Fig. 4). We found from the chemiluminescence assays that esterase-treated MGR1 had in vitro superoxide production comparable to that of JCHD and significantly higher than that of any ROS generator and/or xenobiotic tested at a comparable concentration (Supplementary Fig. 2). We then treated HEK293T cells with MGR1, MGR2, xenobiotics or ROS generators (25 μM for 1 h (1 mM H_2O_2), followed by 10 μM DCF for 10 min), and imaged the cellular fluorescence due to ROS. We found that MGR1 but not MGR2 robustly produced ROS in HEK293T cells, and MGR1 was the best ROS generator, as compared with the other xenobiotics and/or ROS generators (Fig. 1d and Supplementary Fig. 5). Additionally, our prodrug approach of using MGR1 instead of JCHD resulted in more ROS production at the same MGR1 and JCHD concentrations, owing to better MGR1 bioavailability (Supplementary Fig. 5). Similar results were found from other mammalian cell lines (Supplementary Fig. 5). To determine whether the surplus ROS from MGR1 affected cellular viability, we assessed the MGR1 and MGR2 dose dependence on cell death in different mammalian cell lines. In HEK293T cells, we found concentration-dependent cell death after treatment with MGR1 (half-maximal inhibitory concentration (IC_{50}) ~5.7 ± 0.6 μM (mean ± s.e.m.), but not MGR2 (IC_{50} > 40 μM) treatment (Fig. 1e). Similar results were seen in other mammalian cell lines (Supplementary Fig. 6). To confirm that the cell death was ROS dependent, we pretreated mammalian cells with antioxidants, pterostilbene (PTS, 10 μM)[23] or *N*-acetyl-cysteine (NAC, 1 mM)[24], then treated the cells with MGR1 and assessed ROS production. We found that both PTS and NAC substantially decreased the cellular ROS after MGR1 treatment (Supplementary Fig. 7). Additionally, the cell death caused by MGR1 treatment in different mammalian cell lines was also rescued by PTS or NAC, thus further confirming that the lower cellular viability was due to surplus ROS from MGR1 (Supplementary Fig. 8). In subsequent cellular studies, we required a concentration of MGR1 that produced elevated ROS but was not high enough to cause cell death, and chose 2 μM MGR1 or MGR2 (4 h) as the treatment paradigm (Fig. 1e and Supplementary Fig. 6).

A quinone (JCHD) is produced from MGR1, and quinones are known to form covalent adducts with protein thiols[25,26]. To determine the thiol reactivity of MGR1 relative to reactive quinones, we performed gel-based chemoproteomics, using iodoacetamide-alkyne (IAA) as an activity reporter of cellular thiols[27]. In this experiment, HEK293T and RAW264.7 cell lysates were treated with the reactive quinones or MGR1 (+esterase) (all 100 μM, 1 h) and chased with IAA (1 mM, 1 h), after which click reaction was performed[28], and the proteome was resolved and visualized on an SDS–PAGE gel. We found negligible proteome-wide thiol reactivity for MGR1 (or JCHD) relative to reactive quinones (Fig. 1f). Mass spectrometry–based chemoproteomics further confirmed the negligible proteome-wide thiol and serine reactivity of MGR1 (2 μM, 4 h) in HEK293T cells (Supplementary Figs. 9–12 and Supplementary Dataset 1), thus suggesting that the cell death caused by MGR1 was due to surplus ROS and not thiol modification by the quinone product.

Measurement of oxidized PS in cells. Our interest in understanding oxidized-PS metabolism under oxidative stress stemmed from its importance in programmed cell death[12], and we decided to establish an LC–MS/MS method to measure oxidized PS. We first treated C18:0/18:1 PS (1-stearoyl-2-oleoyl-*sn*-glycero-3-phospho-L-serine, 100 μg) with excess H_2O_2 (10 mM) in the presence of iron(II) (1 mM) and ascorbate (1 mM) to produce ROS through Fenton and Haber–Weiss chemistry[29]. We found that, in addition to the native mass of 788.5445 ([M – H]: C18:0/18:1 PS), two new masses of 804.5392 and 806.5549 were present (Fig. 2a). We performed MS/MS on these masses and found that 804.5392 and 806.5549 were +16 (O) and +18 (H_2O) additions, respectively. The MS/MS fragmentations for both these masses suggested that mass additions of +16 (m/z = 297.2431) and +18 (m/z = 299.2590) were present on the *sn*-2 oleate of C18:0/18:1 PS, forming an epoxide and a hydroxide, respectively (Fig. 2a, Supplementary Fig. 13 and Supplementary Note). We denoted the +16 and +18 mass additions with the prefixes ox- and hy-, respectively. We hypothesized that the oxygenation of C18:0/18:1 PS would increase its hydrophilicity, and the resulting oxygenated species would elute earlier on a C18 column. Our observations supported our hypothesis: ox-18:0/18:1 PS and hy-18:0/18:1 PS eluted at 27.8 and 27.1 min, respectively, whereas C18:0/18:1 PS eluted at 32.3 min with our LC–MS/MS method[30] (Fig. 2b). C18:1 lyso-PS eluted at 24.9 min, thus suggesting that both ox-18:0/18:1 PS and hy-18:0/18:1 PS were more lipophilic than C18:1 lyso-PS, because of an additional fatty acid (Fig. 2b). Corroborating the LC–MS/MS findings, thin layer chromatography (TLC)[31] showed a distinct spot for oxidized PS between PS and lyso-PS (Supplementary Fig. 14).

To determine whether MGR1 produces oxidized PS, we treated HEK293T cells with MGR1, MGR2 or DMSO (2 μM, 4 h), and extracted the phospholipids[30,32]. We detected m/z = 788.5445 in all treatment groups, but m/z = 804.5392 and 806.5549 were enriched after MGR1 treatment. To determine whether these masses corresponded to C18:0/18:1 PS, or the synthetic ox-18:0/18:1 PS and hy-18:0/18:1 PS, we performed MS/MS analysis on endogenous m/z = 788.5445, 804.5392 and 806.5549 from phospholipids extracted from MGR1-treated cells. We found that the MS/MS fragmentations for the endogenous masses exactly matched the synthetic standards. Notably, all three masses showed peaks at the parent m/z minus 87.0315 (loss of serine), 437.2671 (1-stearoyl-2-hydroxy-*sn*-glycero-3-phosphate), 419.2562 (dehydro-1-stearoyl-2-hydroxy-*sn*-glycero-3-phosphate), 283.2640 (stearate) and 152.9951 (dehydro-glycerophosphate) (Fig. 2a). We also detected m/z = 297.2433 and 299.2590 in the MS/MS fragmentations of endogenous 804.5392 and 806.5549, respectively, thus confirming the formation of +16 (epoxy) and +18 (hydroxide) oxygenated adducts described earlier for ox-18:0/18:1 PS and hy-18:0/18:1 PS, respectively (Fig. 2a).

The MS/MS fragmentation helped us to develop a targeted multiple reaction monitoring high-resolution (MRM–HR) LC–MS/MS

method to quantify different oxidized-PS species (Supplementary Dataset 2). We validated this method by quantifying ox-18:0/18:1 PS and hy-18:0/18:1 PS from HEK293T cells treated with MGR1, MGR2 or DMSO (2 μM, 4 h), and we found that the MGR1-treated cells had substantially more ox-18:0/18:1 PS and hy-18:0/18:1 PS than MGR2- or DMSO-treated cells, and showed similar elution times to the synthetic standards (Fig. 2c and Supplementary Fig. 13). Next, we measured different ox- and hy-PS after MGR1 and MGR2 treatments in HEK293T cells and found that several ox-PS and hy-PS were significantly elevated after treatment with MGR1 but not MGR2 or DMSO (Fig. 2d). Notably, all detected oxidized PS bore an unsaturated fatty acid esterified at the *sn*-2 position, where the oxygenation probably occurs. We found no changes in cellular PS or lyso-PS, and we were unable to detect oxidized PS secreted from HEK293T cells after treatment with MGR1 or MGR2 (Supplementary Dataset 2). Similar results were observed in other mammalian cell lines (Supplementary Fig. 15 and Supplementary Dataset 2).

Chemical–genetic screen to identify oxidized-PS lipases. To better understand oxidized-PS metabolism, we developed a screen to identify enzymes that hydrolyze oxidized-PS lipids, by using the aforementioned LC–MS/MS method. At the onset, we hypothesized that a lipase (probably a metabolic SH) would perform this activity[20,33]. Hence, we needed a cell line that expresses many SHs and has high lipid content for our screen. Because public databases[34] have shown that RAW264.7 macrophages fulfill these criteria, we chose this cell line as the candidate for the screen. We collated a focused library of 57 compounds, ranging from specific to broad-spectrum lipase inhibitors[20,33] (Supplementary Dataset 3). We treated RAW264.7 cells with inhibitor (10 μM, 4 h) followed by MGR1 (5 μM, 4 h), after which we extracted cellular phospholipids and analyzed the oxidized PS with targeted LC–MS/MS (Supplementary Fig. 16). We used MGR2 and DMSO as screening controls. We set twofold accumulation in cellular oxidized PS as the threshold for identifying hits from the screen, and we found that most inhibitors had no effect on oxidized PS (effects comparable to those of DMSO after MGR1 treatment). However, three compounds—FP-alkyne, tetrahydrolipstatin (THL, also known as orlistat) and methylarachidonyl fluorophosphonate (MAFP)—showed an increase of more than twofold in cellular oxidized PS (Fig. 3a). Both FP-alkyne and MAFP are broad-spectrum SH inhibitors[20], thus further confirming that the lipase of interest was an SH. Because FP-alkyne and MAFP have several enzyme targets, we focused on THL, because this β-lactone inhibitor potently inhibits only a few SHs[35].

To determine targets of THL in RAW264.7 cells, we used competitive-activity-based protein profiling (ABPP) assays. We treated RAW264.7 cells with THL (10 μM, 4 h), then assessed the membrane and soluble proteomes through competitive gel-based ABPP[32] (Fig. 3b and Supplementary Fig. 17). After THL treatment, we found no activity loss in the soluble proteome, whereas the membrane proteome showed several enzymes whose activity was inhibited. Prominent among these was a SH of ~42 kDa, probably ABHD12, a known THL target[35] (Fig. 3b and Supplementary Fig. 17). Next, we coupled ABPP (by using a biotinylated FP probe, FP-biotin)[36] to LC–MS/MS analysis[32], and identified 34 SHs, of which 12 were inhibited >90% (THL, 10 μM, 4 h). Not surprisingly, there were seven lipases (ABHD6, neuropathy target esterase (PNPLA6), hormone-sensitive lipase (HSL or LIPE), ABHD16A, patatin-like phospholipase domain containing protein 7 (PNPLA7), cytosolic phospholipase A2 (PLA2G4A) and ABHD12) among these targets (Fig. 3c and Supplementary Dataset 4). In addition to these, diacylglycerol lipase beta (DAGLβ) and lipoprotein-associated phospholipase A2 (PLA2G7) are also targets of THL[35]. We detected DAGLβ but unexpectedly did not observe substantial inhibition of DAGLβ (Supplementary Dataset 4). We did not detect PLA2G7 in our experiments. Our chemical–genetic screen included specific inhibitors for most THL targets, and these showed almost no effect on cellular oxidized PS in the screen (KT195, WWL70: ABHD6; palmostatin-B: PNPLA6; BAY, Cay10499: HSL; KC01: ABHD16A; pyrrophenone: PLA2G4A; KT109, KT172: DAGLβ; and darapladib, JMN4: PLA2G7) (Supplementary Dataset 3). This procedure enabled the elimination of most lipase targets of THL, except ABHD12 and PNPLA7, thus suggesting that one of these lipases was likely to be an oxidized-PS lipase. Nonetheless, we overexpressed all the lipase targets of THL in HEK293T cells and tested these lysates for substrate hydrolysis activity against lyso-PS, oxidized PS and PS. Additionally, we tested the SHs ABHD3 (ref. [37]) and PNPLA8 (ref. [38]), because they have been reported to hydrolyze oxidized phospholipids. We found that, among all candidate lipases, ABHD12 was the best candidate, with a hydrolysis rate for oxidized PS more than threefold higher than that of any other lipase (Supplementary Fig. 18). As expected, ABHD12 had robust activity against lyso-PS but not PS[39] (Supplementary Fig. 18), thus suggesting that this enzyme can use both lyso-PS and oxidized PS as substrates in vitro.

Biological validation of ABHD12 as an oxidized-PS lipase. To validate whether ABHD12 was indeed an oxidized-PS lipase, we first generated the catalytically 'dead' S246A mutant of human ABHD12 (hABHD12), then overexpressed S246A hABHD12, wild type (WT) hABHD12 or an empty plasmid (mock) in HEK293T cells. Western blot analysis confirmed that WT hABHD12 and S246A hABHD12 were overexpressed in HEK293T membranes, and gel-based ABPP confirmed that S246A hABHD12 was inactive (Fig. 4a). We also confirmed that WT hABHD12 was potently inhibited by THL[35] (Supplementary Fig. 19). First, membrane lysates from HEK293T cells overexpressing mock, WT hABHD12 or S246A hABHD12 were tested against lyso-PS, oxidized PS or PS;[32,39] we found that WT hABHD12 efficiently hydrolyzed lyso-PS and oxidized PS at

Fig. 2 | Characterization and quantification of oxidized PS in mammalian cells after MGR1 treatment. a, MS/MS fragmentation for the lipid standards (red trace) for C18:0/18:1 PS, ox-18:0/18:1 PS and hy-18:0/18:1 PS, and the corresponding endogenous phospholipids (black trace) of *m/z* 788.5445, 804.5392 and 806.5549 from HEK293T cells treated with MGR1 (2 μM, 4 h). The daughter ions common to all masses from the MS/MS analysis include 152.9951 (dehydo-glycerophosphate), 283.2640 (stearate), 419.2562 (dehydro-1-stearoyl-lysophosphatidic acid) and 437.2671 (1-stearoyl-lysophosphatidic acid), and the [parent *m/z* – 87.0315] peak (loss of serine). The key daughter ions distinguishing the three species (denoted in red text) are 281.2481 (oleate for *m/z* = 788.5445), 297.2431 (oleate +16 AMU for *m/z* = 804.5392) and 299.2590 (oleate +18 AMU for *m/z* = 806.5549). This MS/MS fragmentation study was performed in triplicate and yielded reproducible results. **b**, LC–MS elution profiles for the lipid standards for C18:1 lyso-PS, C18:0/18:1 PS, ox-18:0/18:1 PS and hy-18:0/18:1 PS, showing the higher hydrophilicity of ox-18:0/18:1 PS and hy-18:0/18:1 PS than C18:0/18:1 PS. The LC elution profiles were performed in duplicate and yielded reproducible results. **c**, LC–MS/MS traces (MRM-HR) for ox-18:0/18:1 PS (*m/z* = 804.5) and hy-18:0/18:1 PS (*m/z* = 806.6) extracted from HEK293T cells treated with MGR1 (2 μM), MGR2 (2 μM) or DMSO (all 4 h), showing robust increases for ox-18:0/18:1 PS and hy-18:0/18:1 PS, after treatment with MGR1 but not MGR2 or DMSO. This experiment was performed in triplicate and yielded reproducible results. **d**, Targeted LC–MS/MS MRM-HR measurements of oxidized PS from HEK293T cells treated for 4 h with MGR1 (2 μM), MGR2 (2 μM) or DMSO. Data represent mean ± s.e.m. for 5 independent replicates per group. Student's *t* test (two-tailed): ***$P < 0.001$ versus DMSO group. Dataset 2 shows a complete list of quantified lipids and detailed *P* values.

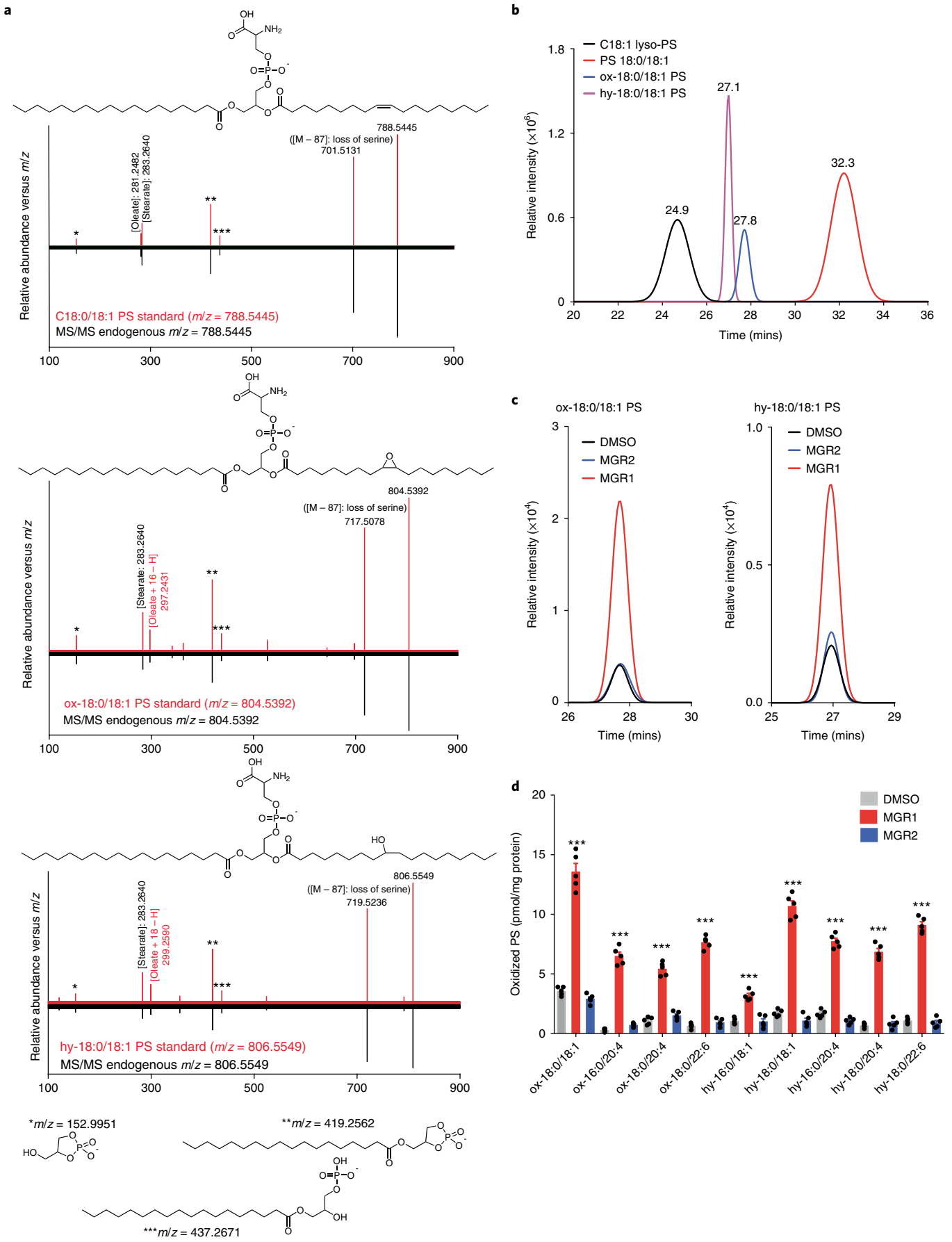
a
Relative abundance versus m/z
788.5445
([M – 87]: loss of serine)
701.5131
[Oleate]: 281.2482
[Stearate]: 283.2640
C18:0/18:1 PS standard (m/z = 788.5445)
MS/MS endogenous m/z = 788.5445
804.5392
717.5078
[Stearate: 283.2640
[Oleate + 16 – H]
297.2431
ox-18:0/18:1 PS standard (m/z = 804.5392)
MS/MS endogenous m/z = 804.5392
806.5549
719.5236
[Stearate]: 283.2640
[Oleate + 18 – H]
299.2590
hy-18:0/18:1 PS standard (m/z = 806.5549)
MS/MS endogenous m/z = 806.5549
*m/z = 152.9951
**m/z = 419.2562
***m/z = 437.2671
b
C18:1 lyso-PS
PS 18:0/18:1
ox-18:0/18:1 PS
hy-18:0/18:1 PS
Relative intensity (×10^6)
27.1
32.3
24.9
27.8
Time (mins)
c
ox-18:0/18:1 PS
hy-18:0/18:1 PS
DMSO
MGR2
MGR1
Relative intensity (×10^4)
Time (mins)
d
DMSO
MGR1
MGR2
Oxidized PS (pmol/mg protein)
ox-18:0/18:1
ox-16:0/20:4
ox-18:0/20:4
ox-18:0/22:6
hy-16:0/18:1
hy-18:0/18:1
hy-16:0/20:4
hy-18:0/20:4
hy-18:0/22:6

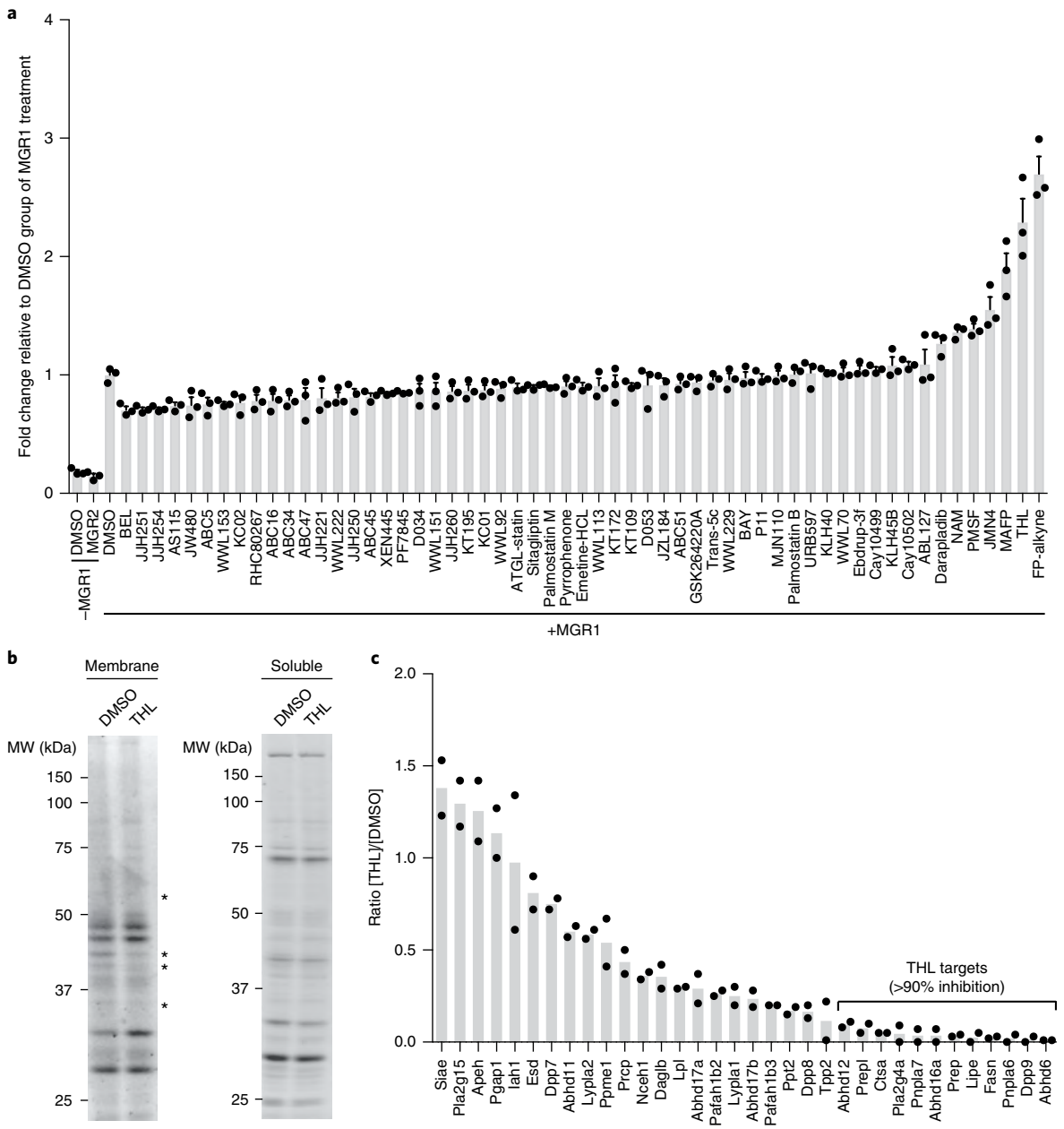

Fig. 3 | Chemical–genetic screen to identify oxidized-PS lipases in mammalian cells. a, Relative oxidized-PS levels from RAW264.7 cells from a highly focused chemical–genetic screen of 57 known lipase inhibitors. Data represent levels relative to those of the DMSO group of MGR1-treated controls. Each group represents mean ± s.e.m. for 3 independent experiments. A twofold increase in oxidized PS was set as a threshold to identify hits in this screen. **b**, ABPP gel of the membrane and soluble proteomes of RAW264.7 cells treated with THL (10 μM, 4 h) or DMSO with FP-rhodamine (2 μM, 37 °C, 45 min). Asterisks represent SH activities inhibited by THL in the membrane proteome. The ABPP gel analyses were performed in triplicate and yielded reproducible results. **c**, ABPP reductive-dimethylation LC–MS/MS analysis for SH activities from RAW264.7 cells treated in situ with THL (10 μM, 4 h). Data represent means for two independent proteomics experiments; each replicate corresponds to the median heavy/light ratio (THL, light; DMSO, heavy) for total quantified peptide for each SH enzyme. A cut off of two or more quantified peptides per SH was required for this analysis. Supplementary Dataset 4 shows the complete ABPP reductive-dimethylation datasets.

comparable rates, but had no activity against PS (Fig. 4b). S246A hABHD12 and mock HEK293T membrane lysates had negligible activity against all three substrates (Fig. 4b). Next, we tested whether heightened ABHD12 activity had any effect on cell viability after MGR1 treatment. Here, HEK293T cells with mock, WT hABHD12 or S246A hABHD12 transfection were treated with MGR1 (0–40 μM, 4 h), and the viable cells were quantified. We found that the mock (IC_{50} = 1.7 ± 0.6 μM) and S246A hABHD12 (IC_{50} = 1.9 ± 0.4 μM) cells had comparable cell-viability profiles after MGR1 treatment, whereas the increased activity of WT hABHD12 partly protected against MGR1 treatment (IC_{50} = 13.9 ± 2.4 μM) (Fig. 4c).

Furthermore, we tested whether overexpression of WT hABHD12 had any effect on cellular oxidized PS. Here, HEK293T cells with mock, WT hABHD12 or S246A hABHD12 transfection were treated with MGR1 (2 μM, 4 h), and cellular oxidized PS was quantified. We found that cells overexpressing WT hABHD12 had significantly lower cellular oxidized PS than did mock- or S246A hABHD12-overexpressing cells (Fig. 4d and Supplementary

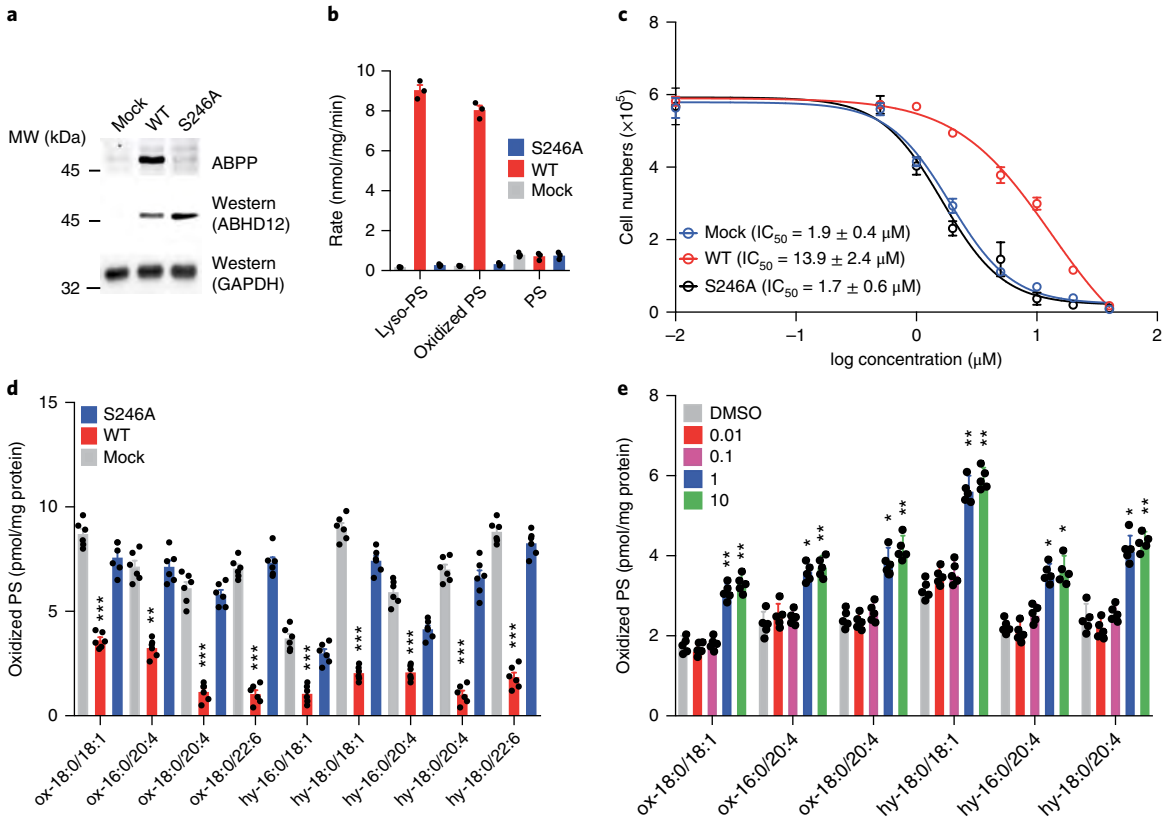

Fig. 4 | Biological validation of human ABHD12 as an oxidized-PS lipase. a, ABPP gel and western blot on the membrane proteomes of HEK293T cells with mock, WT human ABHD12 (hABHD12) or active site S246A hABHD12 mutant transient transfection. The ABPP gel (2 μM FP-rhodamine, 45 min, 37 °C) shows robust activity for WT but not S246A hABHD12 or mock proteomes, whereas the western blot (anti-ABHD12, rabbit, Abcam, 182011) confirms overexpression of WT and S246A hABHD12 over mock. The ABPP gel and western blot analyses were performed in triplicate and yielded reproducible results each time. GAPDH was used as a loading control for these experiments. Full gel images are available in Supplementary Fig. 26. **b**, Substrate assays of membrane proteomes from HEK293T cells with mock, WT or S246A hABHD12 transfection, showing robust hydrolysis of lyso-PS (C18:1) and oxidized PS (ox-C18:0/18:1 PS + hy-18:0/18:1 PS) by the WT but not the S246A hABHD12 or mock proteomes. All proteomes showed negligible activity for the C18:0/18:1 PS. The data represent mean ± s.e.m. for 3 independent experiments. **c**, Cell viability assays on HEK293T cells with mock, WT or S246A hABHD12 transfection, which were treated with increasing concentrations of MGR1 (0–40 μM, 4 h). The results show greater cellular viability for WT hABHD12-transfected HEK293T cells after MGR1 treatment than for mock- or S246A hABHD12-transfected HEK293T cells. Data represent mean ± s.e.m. for 4 independent experiments, and the 95% confidence intervals for the reported IC_{50} values of MGR1 for the mock, WT and S246A groups were 1.5–2.3, 11.5–16.3 and 1.3–2.3 μM, respectively. **d**, Cellular oxidized PS for HEK293T cells with mock, WT or S246A hABHD12 transfection, which were treated with MGR1 (2 μM, 4 h). The WT hABHD12-transfected HEK293T cells had substantially lower oxidized PS than the other groups. Data represent mean ± s.e.m. for 6 independent experiments per group. Student's *t* test (two-tailed): $^{**}P < 0.01$; $^{***}P < 0.001$ versus the mock group. Supplementary Dataset 2 shows a complete list of quantified lipids and detailed *P* values. **e**, Pharmacological blockade of ABHD12 in RAW264.7 cells with increasing THL dosing (0–10 μM, 4 h) causes accumulation in cellular oxidized PS. Data represent mean ± s.e.m. for 5 independent experiments per group. Student's *t* test (two-tailed): $^{*}P < 0.05$; $^{**}P < 0.01$ versus the DMSO group.

Dataset 2), in agreement with the ability of WT hABHD12 but not S246A hABHD12 to hydrolyze oxidized PS. Finally, we tested whether the pharmacological blockade of ABHD12 might have any effect on cellular oxidized PS. In the absence of any reported ABHD12 selective cell active inhibitor, we treated RAW264.7 cells with increasing THL (0–10 μM, 4 h) and found a dose-dependent increase in oxidized PS after THL treatment (Fig. 4e and Supplementary Dataset 2). This result suggests that acute blockade of ABHD12 activity controls cellular oxidized PS.

ABHD12 functions as an oxidized-PS lipase in vivo. To physiologically complement our studies, we first investigated oxidized PS from primary peritoneal macrophages (PPMs) harvested from WT or ABHD12-knockout mice. We found that lipopolysaccharide (LPS) stimulation of PPMs increased the cellular ROS and lyso-PS levels, and ABHD12 controls secreted lyso-PS (Supplementary Figs. 20 and 21 and Supplementary Dataset 2), as previously reported[32,40]. Interestingly, PPMs from WT mice, showed a twofold increase in cellular oxidized PS after LPS stimulation, thus corroborating the increased cellular ROS in PPMs after LPS stimulation[40] (Fig. 5a and Supplementary Dataset 2). Notably, after both vehicle and LPS treatments, PPMs from ABHD12-knockout mice always had approximately twofold more cellular oxidized PS than PPMs from WT mice (Fig. 5a and Supplementary Dataset 2). We did not detect any oxidized-PS secretion from PPMs from either genotype. Next, we tested whether the oxidized PS that we identified might have any role in immunological activation. To assess this possibility, we incubated PPMs from WT or ABHD12-knockout mice with freshly prepared oxidized PS (mixture of ox-18:0/18:1 PS and hy-18:0/18:1 PS), or C18:0/18:1 PS, C18:1 lyso-PS or LPS (all 10 μg/mL, 4 h), then measured the proinflammatory-cytokine secretion from these cells. We found that oxidized PS produced ten- and fivefold more secretion of the cytokines TNF-α and IL-6 in WT PPMs than in the vehicle (or C18:0/18:1 PS) and lyso-PS

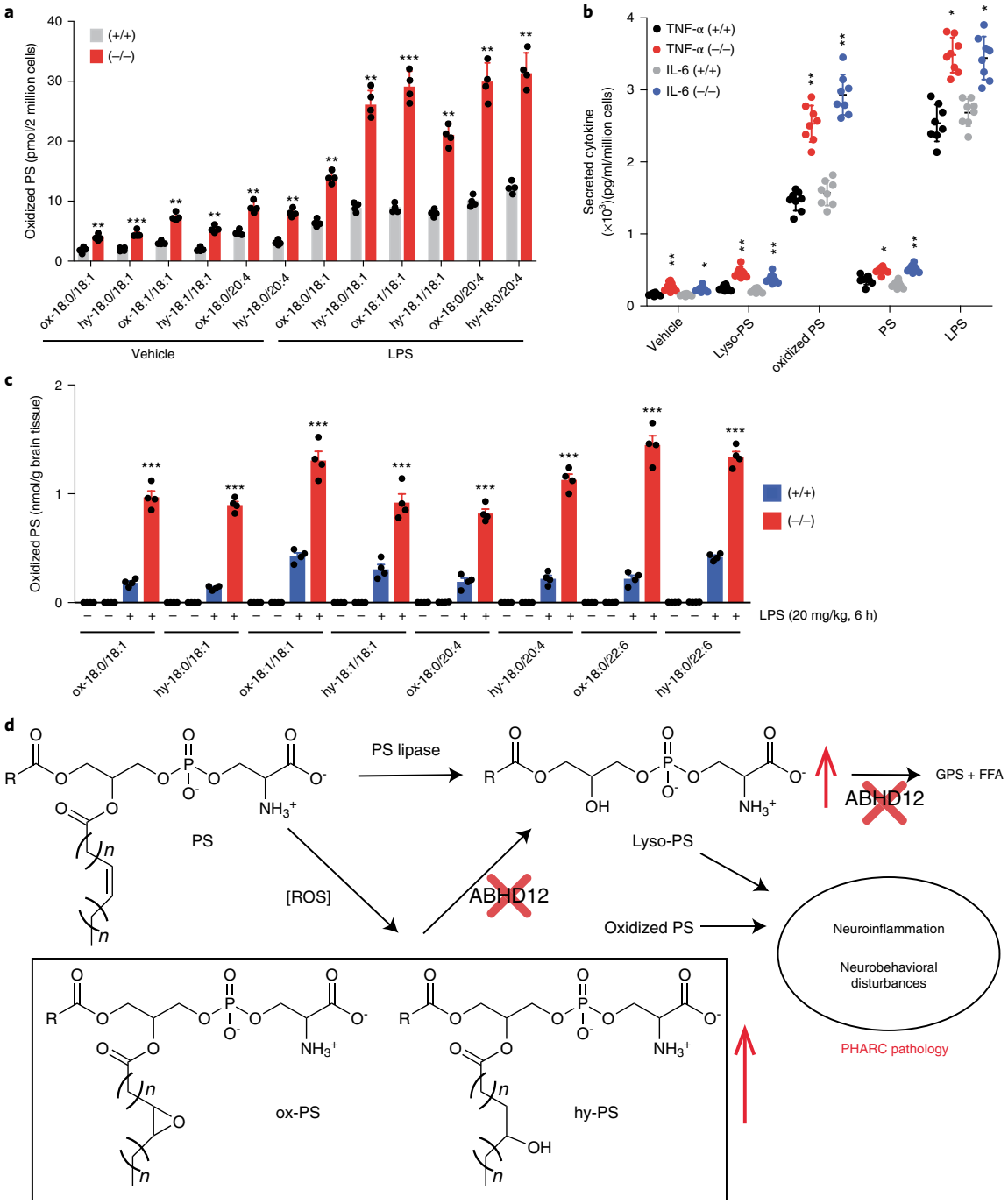

Fig. 5 | ABHD12 functions as an oxidized-PS lipase in vivo. a, Cellular oxidized-PS levels in mouse PPMs harvested from WT (+/+) or ABHD12-knockout (–/–) mice after vehicle (sterile DPBS) or LPS stimulation (10 μg/mL) for 4 h. Data represent mean ± s.e.m. for 4 independent experiments per group. Student's *t* test (two-tailed): $^{**}P < 0.01$; $^{***}P < 0.001$ for the (–/–) versus (+/+) group. Supplementary Dataset 2 shows a complete list of quantified lipids and detailed *P* values. **b**, Secreted concentrations of proinflammatory cytokines TNF-α and IL-6 from mouse PPMs from WT (+/+) and ABHD12-knockout (–/–) mice treated with vehicle (sterile DPBS), C18:1 lyso-PS, oxidized PS (ox-18:0/18:1 PS + hy-18:0/18:1 PS), C18:0/18:1 PS or LPS (10 μg/mL, 4 h). Data represent mean ± s.e.m. for 8 independent experiments per group. Student's *t* test (two-tailed): $^{*}P < 0.05$; $^{**}P < 0.01$ for (–/–) versus (+/+) group. **c**, Oxidized-PS concentrations in the brains of WT (+/+) or ABHD12-knockout (–/–) mice undergoing high-dose acute LPS treatment (20 mg/kg, 6 h, intraperitoneal injections). The data suggest greater accumulation of oxidized PS in the knockout than the WT group in this treatment regime. Data represent mean ± s.e.m. for 4 independent experiments per group. Student's *t* test (two-tailed): $^{**}P < 0.01$; $^{***}P < 0.001$ for the knockout versus WT group. Supplementary Dataset 2 shows a complete list of quantified lipids and detailed *P* values. **d**, Model implicating oxidized-PS lipids in the pathology of the neurological disorder PHARC. Previous studies in a mouse model for PHARC have shown that ABHD12 regulates levels of lyso-PS in the mammalian brain and immune system[32,39], and hence lyso-PS has been attributed to the neuroinflammatory and neurobehavioral disturbances seen in human patients with PHARC[39]. Here, we show that ABHD12 also controls the levels of oxidized PS in different mammalian systems, including primary mouse macrophages and the brain, under oxidative stress. On the basis of previous immunological studies, which suggest a role of oxidized PS in cellular apoptosis, we add to the existing model describing the pathology of PHARC: oxidized PS produced from surplus ROS during oxidative stress may, together with lyso-PS, contribute synergistically to the pathology of this neurological disorder. GPS, glycerophosphoserine; FFA, free fatty acid.

control groups, respectively, and approximately half that in the LPS group (Fig. 5b). When comparing the WT and ABHD12-knockout groups, we found that across all treatments, the PPMs from ABHD12-knockout mice always secreted more TNF-α and IL-6. Notably, oxidized-PS treatment of PPMs from ABHD12-knockout mice showed the greatest response, with approximately twofold greater TNF-α and IL-6 secretion than that of WT PPMs (Fig. 5b). We observed similarly increased proinflammatory-cytokine secretion after oxidized-PS treatment in THP1 macrophages (Supplementary Fig. 22), thus suggesting that oxidized PS is a more potent immunostimulatory lipid than lyso-PS or PS.

Finally, we attempted to analyze oxidized PS in the brains of WT and ABHD12-knockout mice, but were unable to detect it in either genotype. Therefore, we induced neuroinflammation in these mice through intraperitoneal LPS injections with two paradigms[41]—high-dose acute (20 mg/kg, 6 h) and low-dose chronic (1 mg/kg daily for 4 d)—to determine whether oxidized PS was produced, given that these neuroinflammatory LPS stimuli are known to generate enhanced ROS in the mammalian brain[42,43]. We confirmed that the neuroinflammatory challenges were effective by measuring increased prostaglandin and proinflammatory cytokines in the brains of the LPS-treated mice (Supplementary Fig. 23). Interestingly, we found that mice given the the low-dose chronic treatment showed negligible accumulation of oxidized PS, but mice given the high-dose acute treatment showed significant accumulation of oxidized PS in the brain (Fig. 5c and Supplementary Dataset 2). The oxidized-PS accumulation between these genotypes was most pronounced for the high-dose acute treatment, under which the ABHD12-knockout brains accumulated oxidized PS to levels more than fivefold greater than those in similarly treated WT mice (Fig. 5c). We found that the ABHD12-knockout mouse brains always had higher brain lyso-PS content than that in similarly treated WT mouse brains, but the lyso-PS levels did not change during the LPS treatments (Supplementary Fig. 24 and Supplementary Dataset 2). Interestingly, proinflammatory cytokines were also significantly elevated in the ABHD12-knockout brains after high-dose acute LPS treatments (Supplementary Fig. 23).

Discussion

The oxidation of PS due to elevated ROS is linked to its transmembrane migration and presence on the exofacial membrane surface[14,44] (Supplementary Fig. 25), where oxidized-PS externalization generates an 'eat me' signal enabling recognition by phagocytes[12]. An elegant study has shown that apoptotic cells are indeed cleared by macrophages, through specific recognition of externalized oxidized PS by a B-type scavenger receptor[13]. Additionally, the cellular protein annexin-V binds externalized oxidized PS, and several kits for this protein–lipid interaction are available to quantitatively measure apoptotic cells. Whereas PS oxidation and its role in apoptosis are well understood, little is known regarding the enzymatic pathways that metabolize oxidized PS in vivo.

In this study, we sought to identify an enzyme capable of metabolizing oxidized PS in mammalian cells. To this end, we synthesized a chemical probe capable of robustly generating ROS in mammalian cells, thus enabling us to mimic oxidative stress (Fig. 1). Next, we developed an LC–MS/MS method to identify and quantify oxidized PS in mammalian cells, and detected two new oxidized-PS species, termed ox-PS and hy-PS, in different mammalian cells in response to oxidative stress (Fig. 2). We performed a chemical–genetic screen to identify an enzyme capable of metabolizing oxidized PS in mammalian cells and identified ABHD12 as a likely candidate (Fig. 3). We provide compelling biochemical, pharmacological and genetic evidence suggesting that ABHD12 is a major lipase capable of hydrolyzing oxidized PS (Figs 4 and 5).

ABHD12 is of tremendous biomedical interest because it is associated with the human neurodegenerative disease PHARC, which is caused by null mutations to *ABHD12* (refs. [15,16]). ABHD12 is annotated as a lyso-PS lipase in the mammalian brain and immune system[16,32,39,45]. Lipidomic analysis of PPMs from ABHD12-knockout mice[39] and PHARC lymphoblasts from human subjects[16] has indicated that ABHD12 controls levels of secreted lyso-PS but not cellular lyso-PS[32]. This result is not surprising, because the active site of ABHD12 is extracellularly orientated[32,45,46]. It is this active site orientation that, we believe, allows it to access exofacially oriented oxidized PS generated by elevated cellular ROS during oxidative stress (Supplementary Fig. 25). Our studies thus suggest a dual role for ABHD12, in which it regulates cellular oxidized PS and secreted lyso-PS, independently or simultaneously (for example, PPMs). We also found that the newly identified oxidized PS elicits immune responses in PPMs through heightened secretion of proinflammatory cytokines, and the responses are more pronounced in ABHD12-null PPMs. Finally, we determined that ABHD12 controls the levels of oxidized PS in the mammalian brain and in turn the levels of proinflammatory cytokines under severe neuroinflammatory stimuli. Together, our studies build on the existing model describing the progression of PHARC pathology. We propose that, like other neurodegenerative disorders, oxidative stress and ROS may also play roles in PHARC pathology, and, in a basic model, ABHD12 mitigates excess oxidized PS produced in this process (Fig. 5d).

Looking forward, we note that gene expression studies[34] have suggested that ABHD12 is expressed mostly in the nervous and immune systems, yet PS is known to exist in metabolic tissues susceptible to oxidative stress[11]. Hence, resident lipases beyond ABHD12 that metabolize oxidized PS in these tissues must exist. We believe that the tools and methods described here might offer an elegant strategy for functionally annotating such lipases. In addition, developing new tools that enable visualization of oxidized PS in vivo would be beneficial in understanding the spatiotemporal distribution and regulation of these lipids in diverse biological settings. Because the protein ligands and/or receptors for oxidized PS are largely unknown, finding and understanding downstream biological signaling pathways by using emerging chemoproteomics platforms[47,48] would advance the lipid-signaling field and provide new insights into programmed cell death. Finally, recent functional studies have shown that other metabolic SHs are regulators of other oxidized phospholipids in vivo[49,50]. We believe that the emerging functional annotation of orphan SHs might implicate their roles in regulating oxidized lipids from other lipid classes (for example, neutral lipids or sterols) and, in doing so, increase the repertoire of oxidized lipids under oxidative stress.

Online content

Any methods, additional references, Nature Research reporting summaries, source data, statements of data availability and associated accession codes are available at https://doi.org/10.1038/s41589-018-0195-0.

Received: 27 January 2018; Accepted: 9 November 2018;
Published online: 14 January 2019

References

1. Aruoma, O. I. Free radicals, oxidative stress, and antioxidants in human health and disease. *J. Am. Oil. Chem. Soc.* **75**, 199–212 (1998).
2. Niedzielska, E. et al. Oxidative stress in neurodegenerative diseases. *Mol. Neurobiol.* **53**, 4094–4125 (2016).
3. Finkel, T. & Holbrook, N. J. Oxidants, oxidative stress and the biology of ageing. *Nature* **408**, 239–247 (2000).
4. Liou, G. Y. & Storz, P. Reactive oxygen species in cancer. *Free. Radic. Res.* **44**, 479–496 (2010).
5. Imlay, J. A. The molecular mechanisms and physiological consequences of oxidative stress: lessons from a model bacterium. *Nat. Rev. Microbiol.* **11**, 443–454 (2013).
6. Porter, N. A. A perspective on free radical autoxidation: the physical organic chemistry of polyunsaturated fatty acid and sterol peroxidation. *J. Org. Chem.* **78**, 3511–3524 (2013).

7. Yin, H., Xu, L. & Porter, N. A. Free radical lipid peroxidation: mechanisms and analysis. *Chem. Rev.* **111**, 5944–5972 (2011).
8. Spickett, C. M. & Pitt, A. R. Oxidative lipidomics coming of age: advances in analysis of oxidized phospholipids in physiology and pathology. *Antioxid. Redox. Signal.* **22**, 1646–1666 (2015).
9. Smith, W. L. & Murphy, R. C. Oxidized lipids formed non-enzymatically by reactive oxygen species. *J. Biol. Chem.* **283**, 15513–15514 (2008).
10. Vance, J. E. & Tasseva, G. Formation and function of phosphatidylserine and phosphatidylethanolamine in mammalian cells. *Biochim. Biophys. Acta* **1831**, 543–554 (2013).
11. Leventis, P. A. & Grinstein, S. The distribution and function of phosphatidylserine in cellular membranes. *Annu. Rev. Biophys.* **39**, 407–427 (2010).
12. Hazen, S. L. Oxidized phospholipids as endogenous pattern recognition ligands in innate immunity. *J. Biol. Chem.* **283**, 15527–15531 (2008).
13. Greenberg, M. E. et al. Oxidized phosphatidylserine-CD36 interactions play an essential role in macrophage-dependent phagocytosis of apoptotic cells. *J. Exp. Med.* **203**, 2613–2625 (2006).
14. Kagan, V. E. et al. A role for oxidative stress in apoptosis: oxidation and externalization of phosphatidylserine is required for macrophage clearance of cells undergoing Fas-mediated apoptosis. *J. Immunol.* **169**, 487–499 (2002).
15. Fiskerstrand, T. et al. Mutations in ABHD12 cause the neurodegenerative disease PHARC: an inborn error of endocannabinoid metabolism. *Am. J. Hum. Genet.* **87**, 410–417 (2010).
16. Chen, D. H. et al. Two novel mutations in ABHD12: expansion of the mutation spectrum in PHARC and assessment of their functional effects. *Hum. Mutat.* **34**, 1672–1678 (2013).
17. Dharmaraja, A. T. & Chakrapani, H. A small molecule for controlled generation of reactive oxygen species (ROS). *Org. Lett.* **16**, 398–401 (2014).
18. Dharmaraja, A. T., Alvala, M., Sriram, D., Yogeeswari, P. & Chakrapani, H. Design, synthesis and evaluation of small molecule reactive oxygen species generators as selective Mycobacterium tuberculosis inhibitors. *Chem. Commun. (Camb).* **48**, 10325–10327 (2012).
19. Tyagi, P., Dharmaraja, A. T., Bhaskar, A., Chakrapani, H. & Singh, A. *Mycobacterium tuberculosis* has diminished capacity to counteract redox stress induced by elevated levels of endogenous superoxide. *Free Radic. Biol. Med.* **84**, 344–354 (2015).
20. Long, J. Z. & Cravatt, B. F. The metabolic serine hydrolases and their functions in mammalian physiology and disease. *Chem. Rev.* **111**, 6022–6063 (2011).
21. Huu, T. P., Marquetty, C., Pasquier, C. & Hakim, J. Luminol assay for microdetermination of superoxide dismutase activity: its application to human fetal blood. *Anal. Biochem.* **142**, 467–472 (1984).
22. Zhao, H. et al. Detection and characterization of the product of hydroethidine and intracellular superoxide by HPLC and limitations of fluorescence. *Proc. Natl. Acad. Sci. USA* **102**, 5727–5732 (2005).
23. McCormack, D. & McFadden, D. A review of pterostilbene antioxidant activity and disease modification. *Oxid. Med. Cell Longev.* **2013**, 575482 (2013).
24. Kerksick, C. & Willoughby, D. The antioxidant role of glutathione and N-acetyl-cysteine supplements and exercise-induced oxidative stress. *J. Int. Soc. Sports. Nutr.* **2**, 38–44 (2005).
25. Liebeke, M. et al. Depletion of thiol-containing proteins in response to quinones in *Bacillus subtilis*. *Mol. Microbiol.* **69**, 1513–1529 (2008).
26. O'Brien, P. J. Molecular mechanisms of quinone cytotoxicity. *Chem. Biol. Interact.* **80**, 1–41 (1991).
27. Weerapana, E. et al. Quantitative reactivity profiling predicts functional cysteines in proteomes. *Nature* **468**, 790–795 (2010).
28. Speers, A. E., Adam, G. C. & Cravatt, B. F. Activity-based protein profiling in vivo using a copper(i)-catalyzed azide-alkyne [3+2] cycloaddition. *J. Am. Chem. Soc.* **125**, 4686–4687 (2003).
29. Zschörnig, K. & Schiller, J. A simple method to generate oxidized phosphatidylcholines in amounts close to one milligram. *Chem. Phys. Lipids* **184**, 30–37 (2014).
30. Pathak, D., Mehendale, N., Singh, S., Mallik, R. & Kamat, S. S. Lipidomics suggests a new role for ceramide synthase in phagocytosis. *ACS Chem. Biol.* **13**, 2280–2287 (2018).
31. Knittelfelder, O. L. & Kohlwein, S. D. Thin-layer chromatography to separate phospholipids and neutral lipids from yeast. *Cold Spring Harb. Protoc.* **2017**, pdb.prot085456 (2017).
32. Kamat, S. S. et al. Immunomodulatory lysophosphatidylserines are regulated by ABHD16A and ABHD12 interplay. *Nat. Chem. Biol.* **11**, 164–171 (2015).
33. Nomura, D. K. & Casida, J. E. Lipases and their inhibitors in health and disease. *Chem. Biol. Interact.* **259**, 211–222 (2016).
34. Wu, C., Jin, X., Tsueng, G., Afrasiabi, C. & Su, A. I. BioGPS: building your own mash-up of gene annotations and expression profiles. *Nucleic Acids Res.* **44**, D313–D316 (2016).
35. Hoover, H. S., Blankman, J. L., Niessen, S. & Cravatt, B. F. Selectivity of inhibitors of endocannabinoid biosynthesis evaluated by activity-based protein profiling. *Bioorg. Med. Chem. Lett.* **18**, 5838–5841 (2008).
36. Liu, Y., Patricelli, M. P. & Cravatt, B. F. Activity-based protein profiling: the serine hydrolases. *Proc. Natl. Acad. Sci. USA* **96**, 14694–14699 (1999).
37. Long, J. Z. et al. Metabolomics annotates ABHD3 as a physiologic regulator of medium-chain phospholipids. *Nat. Chem. Biol.* **7**, 763–765 (2011).
38. Ramanadham, S. et al. Calcium-independent phospholipases A2 and their roles in biological processes and diseases. *J. Lipid Res.* **56**, 1643–1668 (2015).
39. Blankman, J. L., Long, J. Z., Trauger, S. A., Siuzdak, G. & Cravatt, B. F. ABHD12 controls brain lysophosphatidylserine pathways that are deregulated in a murine model of the neurodegenerative disease PHARC. *Proc. Natl. Acad. Sci. USA* **110**, 1500–1505 (2013).
40. Hsu, H. Y. & Wen, M. H. Lipopolysaccharide-mediated reactive oxygen species and signal transduction in the regulation of interleukin-1 gene expression. *J. Biol. Chem.* **277**, 22131–22139 (2002).
41. Viader, A. et al. A chemical proteomic atlas of brain serine hydrolases identifies cell type-specific pathways regulating neuroinflammation. *eLife* **5**, e12345 (2016).
42. You, L. H. et al. Astrocyte hepcidin is a key factor in LPS-induced neuronal apoptosis. *Cell Death Dis.* **16**, e2676 (2017).
43. Hou, C. et al. Development of a positron emission tomography radiotracer for imaging elevated levels of superoxide in neuroinflammation. *ACS Chem. Neurosci.* **9**, 578–586 (2018).
44. Matsura, T. et al. The presence of oxidized phosphatidylserine on Fas-mediated apoptotic cell surface. *Biochim. Biophys. Acta* **1736**, 181–188 (2005).
45. Joshi, A. et al. Biochemical characterization of the PHARC-associated serine hydrolase ABHD12 reveals its preference for very-long-chain lipids. *J. Biol. Chem.* **293**, 16953–16963 (2018).
46. Blankman, J. L., Simon, G. M. & Cravatt, B. F. A comprehensive profile of brain enzymes that hydrolyze the endocannabinoid 2-arachidonoylglycerol. *Chem. Biol.* **14**, 1347–1356 (2007).
47. Niphakis, M. J. et al. A global map of lipid-binding proteins and their ligandability in cells. *Cell* **161**, 1668–1680 (2015).
48. Hulce, J. J., Cognetta, A. B., Niphakis, M. J., Tully, S. E. & Cravatt, B. F. Proteome-wide mapping of cholesterol-interacting proteins in mammalian cells. *Nat. Methods* **10**, 259–264 (2013).
49. Rosenson, R. S. & Stafforini, D. M. Modulation of oxidative stress, inflammation, and atherosclerosis by lipoprotein-associated phospholipase A2. *J. Lipid Res.* **53**, 1767–1782 (2012).
50. Shimanaka, Y. et al. Omega-3 fatty acid epoxides are autocrine mediators that control the magnitude of IgE-mediated mast cell activation. *Nat. Med.* **23**, 1287–1297 (2017).

Acknowledgements

This work was supported by grants from the Wellcome Trust DBT India Alliance (IA/I/15/2/502058 to S.S.K.), DST-SERB (ECR/2016/001261 to S.S.K.; EMR/2015/000668 to H.C.), DBT (BT/PR15848/MED/29/1025/2016 to H.C.) and DST-FIST (Infrastructure Development to IISER Pune Biology Department). B. F. Cravatt (The Scripps Research Institute) is thanked for providing chemical compounds, inhibitors and ABHD12-knockout mice used in this study, and for insightful comments on the manuscript. N. Balasubramanian (IISER Pune) is thanked for access to the EVOS Imaging System for the cellular fluorescence experiments. The National Facility for Gene Function in Health and Disease, IISER Pune, is thanked for maintaining and providing mice for this study. G.R., A.K.S. and A.R. acknowledge research fellowships from the Council for Scientific and Industrial Research (CSIR), Government of India, and N.M. acknowledges a research fellowship from DBT, Government of India.

Author contributions

D.S.K., N.M., S.S., A.J., A.R. and S.S.K. performed the biochemical experiments and analyzed the data. G.R., A.K.S., A.M. and H.C. synthesized and chemically characterized all the chemical compounds in this study. D.S.K. and S.S.K. performed and analyzed the proteomics data. S.S.K. and H.C. conceived the project and designed the experiments. S.S.K. wrote the paper, to which all authors provided input.

Competing interests

The authors declare no competing interests.

Additional information

Supplementary information is available for this paper at https://doi.org/10.1038/s41589-018-0195-0.

Reprints and permissions information is available at www.nature.com/reprints.

Correspondence and requests for materials should be addressed to S.S.K.

Publisher's note: Springer Nature remains neutral with regard to jurisdictional claims in published maps and institutional affiliations.

Cell Chemical Biology

CellPress

Article

Fatty acid chain length drives lysophosphatidylserine-dependent immunological outputs

Neha Khandelwal,[1,5] Minhaj Shaikh,[2,5] Amol Mhetre,[1,5,*] Shubham Singh,[1,5] Theja Sajeevan,[1] Alaumy Joshi,[1,4] Kithiganahalli Narayanaswamy Balaji,[3] Harinath Chakrapani,[2,*] and Siddhesh S. Kamat[1,6,*]

[1]Department of Biology, Indian Institute of Science Education and Research (IISER) Pune, Dr. Homi Bhabha Road, Pashan, Pune, Maharashtra 411008, India

[2]Department of Chemistry, Indian Institute of Science Education and Research (IISER) Pune, Dr. Homi Bhabha Road, Pashan, Pune, Maharashtra 411008, India

[3]Department of Microbiology and Cell Biology, Indian Institute of Science (IISc), Bangalore, Karnataka 560012, India

[4]Present address: Department of Biochemistry & Biophysics, Texas A&M University, College Station, TX 77843, USA

[5]These authors contributed equally

[6]Lead contact

*Correspondence: amol@iiserpune.ac.in (A.M.), harinath@iiserpune.ac.in (H.C.), siddhesh@iiserpune.ac.in (S.S.K.)

https://doi.org/10.1016/j.chembiol.2021.01.008

SUMMARY

In humans, lysophosphatidylserines (lyso-PSs) are potent lipid regulators of important immunological processes. Given their structural diversity and commercial paucity, here we report the synthesis of methyl esters of lyso-PS (Me-lyso-PSs) containing medium- to very-long-chain (VLC) lipid tails. We show that Me-lyso-PSs are excellent substrates for the lyso-PS lipase ABHD12, and that these synthetic lipids are acted upon by cellular carboxylesterases to produce lyso-PSs. Next, in macrophages we demonstrate that VLC lyso-PSs orchestrate pro-inflammatory responses and in turn neuroinflammation via a Toll-like receptor 2 (TLR2)-dependent pathway. We also show that long-chain (LC) lyso-PSs robustly induce intracellular cyclic AMP production, cytosolic calcium influx, and phosphorylation of the nodal extracellular signal-regulated kinase to regulate macrophage activation via a TLR2-independent pathway. Finally, we report that LC lyso-PSs potently elicit histamine release during the mast cell degranulation process, and that ABHD12 is the major lyso-PS lipase in these immune cells.

INTRODUCTION

Lipids have long been known as potent signaling molecules that mediate many important physiological processes in mammals, including humans (Wymann and Schneiter, 2008; Dennis, 2016; Fahy et al., 2005). Prominent among the signaling lipids are the prostaglandins (Dennis and Norris, 2015), the endocannabinoids (2-arachidonoylglycerol [2-AG] and anandamide [AEA]) (Blankman and Cravatt, 2013; Fowler et al., 2005), and the well-studied lysophospholipids, sphingosine 1-phosphate (S1P) (Gonzalez-Cabrera et al., 2014; Rosen et al., 2013) and lysophosphatidic acid (lyso-PA) (Ishii et al., 2004; Contos et al., 2000). Given their physiological importance, the biosynthetic/degradative enzyme(s) and/or cognate receptor(s) of the aforementioned lysophospholipids (S1P and lyso-PA) are pharmacological targets for drugs already in clinical use or under investigation in different phases of clinical trials for an array of human neurological and immunological disorders (Gardell et al., 2006; Yanagida and Valentine, 2020). Recently, the lysophosphatidylserines (lyso-PSs) have emerged as yet another important class of signaling lysophospholipids (Shanbhag et al., 2020), with potent bioactivities in the mammalian central nervous and immune system.

Cellular pharmacological studies have shown that lyso-PSs regulate several immunological processes (Shanbhag et al., 2020) such as macrophage activation to clear apoptotic cells (Frasch and Bratton, 2012), mast cell degranulation (Lloret and Moreno, 1995), leukemic cell stimulation (Park et al., 2005), chemotaxis of human gliomas (Lee et al., 2008), and maturation of regulatory T cells (Barnes et al., 2015), and perhaps signal through Toll-like receptors (TLRs) (Van Der Kleij et al., 2002) and/or G-protein-coupled receptors (GPCRs) (Inoue et al., 2012) in the mammalian nervous and immune system. Interestingly, and of biomedical relevance, mutations to the putative lyso-PS receptors in humans have been linked to different autoimmune diseases (Szymanski et al., 2014; Napier et al., 2015; Chu et al., 2013). Murine studies have recently shown that accumulation of lyso-PS, especially very-long-chain (VLC) lyso-PSs (Blankman et al., 2013), in the mammalian brain is a major cause that drives the pathology of the early-onset human neurological disorder PHARC (polyneuropathy, hearing loss, ataxia, retinitis pigmentosa, and cataract) (Fiskerstrand et al., 2009, 2010).

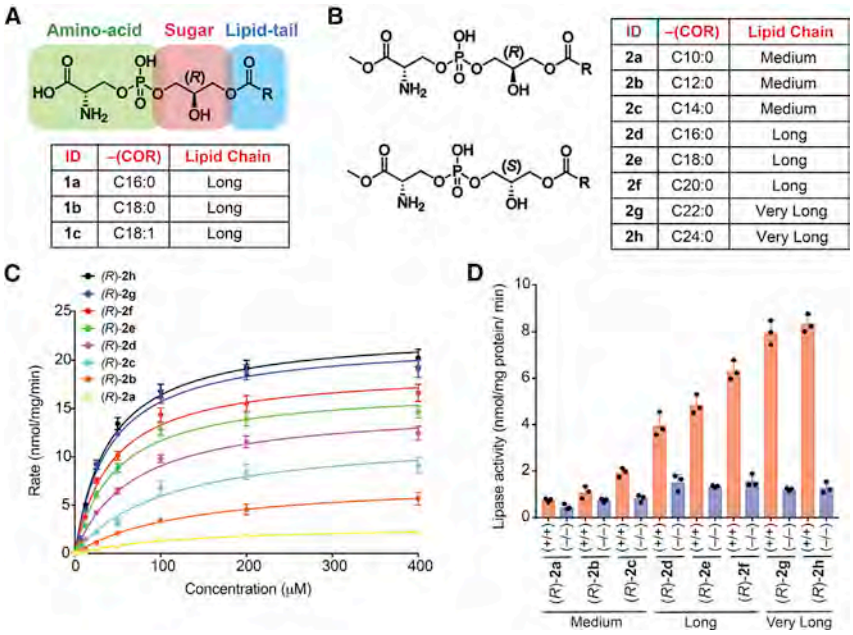

ID	–(COR)	Lipid Chain
1a	C16:0	Long
1b	C18:0	Long
1c	C18:1	Long

ID	–(COR)	Lipid Chain
2a	C10:0	Medium
2b	C12:0	Medium
2c	C14:0	Medium
2d	C16:0	Long
2e	C18:0	Long
2f	C20:0	Long
2g	C22:0	Very Long
2h	C24:0	Very Long

Figure 1. Structure of Me-lyso-PSs, and testing them as substrates against ABHD12

(A and B) The chemical structures of (A) commercially available canonical natural lyso-PSs and (B) our synthetic Me-lyso-PS lipid library with both (*R*)- and (*S*)-stereoisomers.

(C) Enzyme kinetic assays for membrane lysates (10 μg) of HEK293T cells transfected with hABHD12 tested against the (*R*)-Me-lyso-PSs (0–400 μM, 30 min, 37°C, n = 3/data point). The line connecting the points represents a fit to the Michaelis-Menten enzyme kinetics equation. See Table 1 for all enzyme kinetics parameters.

(D) Lipase assays for (*R*)-Me-lyso-PSs (100 μM, 30 min, 37°C, n = 3/group) tested against brain membrane lysates (20 μg) from wild-type (WT) (+/+) or ABHD12 knockout (−/−) mice. All data presented in (C) (data points) and (D) (bars) are presented as mean ± standard deviation (SD).

Interestingly, PHARC is caused by deleterious mutations to the *abhd12* gene (Fiskerstrand et al., 2009, 2010), which encodes an integral membrane metabolic serine hydrolase ABHD12 (α/β hydrolase domain-containing protein 12), a major and, to date, only *in vivo* functionally characterized lyso-PS lipase (Kamat et al., 2015; Blankman et al., 2013; Singh et al., 2020).

Given the strong link between lyso-PSs and human diseases, mechanistic studies are much needed to understand in more detail and biochemically characterize the signaling pathways influenced by lyso-PSs *in vivo*. Two factors complicate and/or limit such studies: (1) unlike other signaling lipids (e.g., S1P, 2-AG, AEA), *in vivo* lyso-PSs are found esterified with different fatty acids (ranging from medium-chain [C10] to VLC [C24]) (Blankman et al., 2013; Barnes et al., 2015), and hence the precise physiological contributions of the individual lyso-PSs remain cryptic; (2) commercially, lyso-PSs are limited, and even those that are available are esterified only with long-chain (LC) fatty acids (C16:0, C18:0, and C18:1) (Figure 1A). Therefore, delineating the biological contributions of medium or VLC lyso-PSs has not been possible to date.

To address the aforementioned problems, here we describe the synthesis of methyl esters of lyso-PS (Me-lyso-PS) bearing fatty acids of varying chain lengths ranging from medium-chain (C10–C14) to LC (C16–C20) to VLC (>C20) having the canonical natural (*R*)- or unnatural (*S*)-configuration at the glycerol backbone. Next, we test these synthetic Me-lyso-PS lipids in a variety of biological assays, and show that the canonical (*R*)-Me-lyso-PSs are highly bioactive while the corresponding unnatural (*S*)-Me-lyso-PSs are largely inactive. Specifically, we show that (*R*)-Me-lyso-PS are excellent substrates for the PHARC-associated lyso-PS lipase ABHD12, and confirm this enzyme's preference for VLC lyso-PS lipids (Joshi et al., 2018; Kamat et al., 2015; Blankman et al., 2013). Furthermore, we show that cellular carboxylesterases hydrolyze the methyl-ester moiety of Me-lyso-PSs to yield lyso-PSs, and thus demonstrate that the synthetic Me-lyso-PSs serve as stable prodrug-like biological precursors to lyso-PSs. Of note, we report the distinct contribution of individual lyso-PS lipids in activation and pro-inflammatory responses from macrophages and in the release of histamine during mast cell degranulation, and specifically show how the fatty acid chain length of lyso-PSs plays a critical role in the output of the aforementioned important immunological processes. Finally, we also annotate the metabolic serine hydrolase ABHD12 as a major lyso-PS lipase in primary mast cells, and expand the possible physiological role of this biomedically important lipase to an additional immunological process.

RESULTS

Synthesis of Me-lyso-PS lipids

Structurally, lyso-PSs are composed of three building blocks: (1) a sugar backbone (glycerol), (2) an amino acid head group (phospho-L-serine), and (3) a lipid tail (fatty acid) (Figure 1A) (Fahy et al., 2011). It is this intricate combination of hydrophilic (glycerol and phospho-L-serine) and hydrophobic (fatty acid) biological building blocks that confers amphiphilic properties to lyso-PSs and enables them to access different cellular membranes, organelles, and compartments. Given this amphiphilic property, lyso-PSs serve as potent hormone-like mediators of various important immunological processes (Vance, 2015; Tracey et al., 2018; Shanbhag et al., 2020). From a stereochemical perspective, all natural lyso-PSs have two chiral centers: (1) α-carbon of the phospho-L-serine head group and (2) *sn-2* carbon of the (*R*)-glycerol backbone (Figure 1A) (Mallik et al., 2018). Biosynthetically, lyso-PSs are made from phosphatidylserine (PS) precursors, by the enzymatic action of PS-specific phospholipases (Hosono et al., 2001; Kamat et al., 2015), and subsequent studies have shown that physiologically, almost all lyso-PSs exists as 1-(fatty acyl)-2-hydroxy-*sn*-glycero-3-phospho-L-serine (Iwashita et al., 2009; Kamat et al., 2015). Given the synthetic challenges in making this bioactive lipid, for example, (1) combination of the aforementioned hydrophilic and hydrophobic moieties, (2) lipophilicity of the final molecule, and (3) the need for retention in configuration of the two chiral centers toward making the correct diastereomer,

Table 1. Kinetic constants for lyso-PS and Me-lyso-PS substrates tested against hABHD12 (HEK293T membrane lysates transiently transfected with hABHD12)

Lyso-PS species	Fatty acid chain length: unsaturation	V_{max} (nmol/mg protein/min)	K_M (μM)	V_{max}/K_M (nmol/mg protein/min/M) (× 10^5)
1a	16:0	15.6 ± 0.6	72 ± 8	2.2 ± 0.3
1b	18:0	18.3 ± 0.5	48 ± 4	3.8 ± 0.4
1c	18:1	17.8 ± 0.6	46 ± 6	3.8 ± 0.5
(*R*)-**2a**	10:0	2.9 ± 0.2	126 ± 18	0.2 ± 0.04
(*R*)-**2b**	12:0	7.6 ± 0.3	131 ± 14	0.6 ± 0.06
(*R*)-**2c**	14:0	12.2 ± 0.6	106 ± 14	1.1 ± 0.1
(*R*)-**2d**	16:0	15.2 ± 0.6	67 ± 7	2.3 ± 0.3
(*R*)-**2e**	18:0	17.2 ± 0.6	47 ± 5	3.7 ± 0.5
(*R*)-**2f**	20:0	19.0 ± 0.6	43 ± 4	4.4 ± 0.5
(*R*)-**2g**	22:0	22.0 ± 0.6	40 ± 4	5.5 ± 0.6
(*R*)-**2h**	24:0	22.9 ± 0.6	40 ± 4	5.7 ± 0.6
(*S*)-**2a**	10:0	0.2 ± 0.02	275 ± 32	0.007 ± 0.001
(*S*)-**2b**	12:0	0.4 ± 0.05	255 ± 35	0.016 ± 0.002
(*S*)-**2c**	14:0	0.6 ± 0.1	215 ± 28	0.028 ± 0.003
(*S*)-**2d**	16:0	0.8 ± 0.1	187 ± 24	0.043 ± 0.006
(*S*)-**2e**	18:0	1.2 ± 0.1	178 ± 25	0.067 ± 0.008
(*S*)-**2f**	20:0	1.3 ± 0.2	165 ± 23	0.078 ± 0.009
(*S*)-**2g**	22:0	1.2 ± 0.2	167 ± 26	0.072 ± 0.009
(*S*)-**2h**	24:0	1.2 ± 0.3	176 ± 31	0.068 ± 0.008

only three naturally occurring LC lyso-PSs (**1a–1c**) are commercially available, thus limiting any rigorous structure-activity relationship (SAR) studies for this important lysophospholipid class (Figure 1A). Since the commercial paucity of lyso-PSs would impede our proposed studies, here we describe a facile synthesis route toward making Me-lyso-PS esterified with saturated fatty acids of varying chain lengths ranging from medium-chain to VLC (Figure 1B and Data S1). Speculating that the free reactive carboxylate moiety of the amino acid end of the molecule might cross-react and complicate the synthesis, we decided to make the Me-lyso-PS version. Our synthetic route successfully afforded the naturally occurring canonical (*R*)-Me-lyso-PSs (Figure 1B and Data S1) and the unnatural (*S*)-Me-lyso-PSs (Figure 1B and Data S1) with the same fatty acids (Figure 1B) to yield final compounds ((*R*)-**2a–2h** or (*S*)-**2a–2h**) in milligram quantities.

ABHD12 prefers VLC lyso-PSs as substrates

The lipids previously tested as substrates for the mammalian lyso-PS lipase ABHD12 have been commercially available LC lyso-PSs (**1a–1c**) (Blankman et al., 2013; Kamat et al., 2015) (Figure 1A) and various monoacylglycerol (MAG) lipids (Blankman et al., 2007; Joshi et al., 2018; Navia-Paldanius et al., 2012). In the absence of a commercial source for medium or VLC lyso-PSs, which to the best of our knowledge have not been tested against ABHD12, the MAG lipids have served as excellent surrogates for performing SAR studies toward biochemically understanding the substrate preference for this lipase (Joshi et al., 2018). Therefore, having synthesized the library of (*R*)- and (*S*)-Me-lyso-PSs containing medium-chain, LC, and VLC variants (nomenclature in Figure 1B), we first wanted to test whether these lipids were indeed substrates for ABHD12. Leveraging established liquid chromatography coupled with mass spectrometry (LC-MS)-based substrate assays (Joshi et al., 2018), we found that both recombinant human ABHD12 (hABHD12) (Table 1 and Figure S1A) and endogenous mouse brain ABHD12 (mABHD12) (Figure S1B) robustly turned over (*R*)-Me-lyso-PSs, and for the same fatty acid, LC (*R*)-Me-lyso-PS and corresponding canonical natural LC lyso-PS behaved almost identically. Next, we performed rigorous enzyme kinetics measurements for our (*R*)-Me-lyso-PS library against hABHD12 (Figure 1C and Table 1) and found that hABHD12 strongly prefers VLC (*R*)-Me-lyso-PSs as substrates, with (*R*)-**2h** (C24:0, V_{max} = 22.9 ± 0.6 nmol/mg protein/min, K_M = 40 ± 4 μM) and (*R*)-**2g** (C22:0, V_{max} = 22.0 ± 0.6 nmol/mg protein/min, K_M = 40 ± 4 μM) being the best substrates. Furthermore, mouse brain membrane lysates were assayed against the same Me-lyso-PS library, and here too we found that mABHD12 strongly prefers VLC (*R*)-Me-lyso-PSs, with (*R*)-**2h** (C24:0, rate = 8.2 ± 0.3 nmol/mg protein/min) and (*R*)-**2g** (C22:0, rate = 8.0 ± 0.3 nmol/mg protein/min) being the best substrates (Figure 1D). In this experiment, mouse brain membrane lysates from ABHD12-null mice were used as controls to delineate specific contributions from mABHD12 (Figure 1D). In both these assays, we also tested (*S*)-Me-lyso-PSs and found, not surprisingly, that these were very poor substrates for hABHD12 (Table 1 and Figure S1C) and mABHD12 (Figure S1D), with catalytic efficiencies 100-fold lower than that of corresponding (*R*)-Me-lyso-PSs for hABHD12 (Table 1). Taken together, these substrate assays conclusively show that the ABHD12-catalyzed lyso-PS lipase reaction is highly stereospecific, prefers VLC (*R*)-lyso-PSs as substrates, and, together with recent findings (Singh et al., 2020; Joshi et al., 2018), now provides a concrete biochemical explanation as to why VLC lyso-PSs accumulate the most in ABHD12 knockout mouse brains (Blankman et al., 2013).

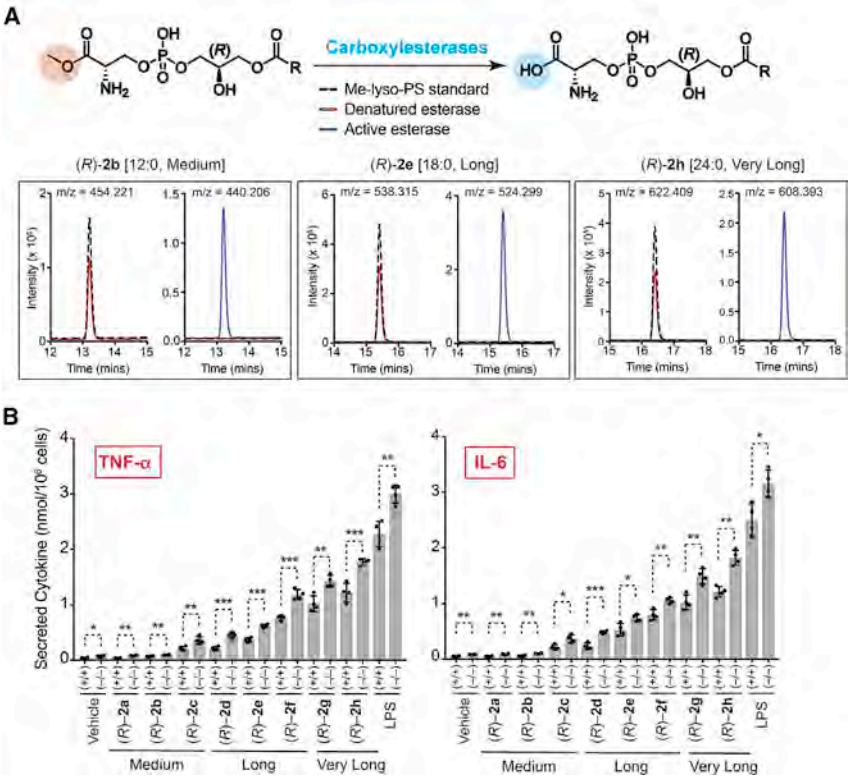

Figure 2. Metabolism of Me-lyso-PSs by carboxylesterases and the pro-inflammatory activity of Me-lyso-PSs in macrophages

(A) Top: the enzymatic reaction for metabolism (hydrolysis) of Me-lyso-PSs to the corresponding lyso-PSs catalyzed by carboxylesterases. Bottom: extracted ion chromatograms from a LC-MS analysis of (*R*)-**2b** (C12:0) ($[M-H]^-$ = 454.221), (*R*)-**2e** (C18:0) ($[M-H]^-$ = 538.315), and (*R*)-**2h** (C24:0) ($[M-H]^-$ = 622.409) showing the complete conversion of the parent compound (Me-lyso-PS) to the corresponding lyso-PS (loss of 14 Da) following treatment with active (blue trace), but not denatured (red trace), porcine liver carboxylesterase (0.1 U, 15 min, 37°C). In these assays, 100 μg of the (*R*)-Me-lyso-PS was used, and a no-enzyme standard only control (dotted black trace) was also included for the same treatment. This LC-MS experiment was done twice for each of the (*R*)-Me-lyso-PS, with reproducible results each time.

(B) Secreted TNF-α and IL-6 from PPMs harvested from WT (+/+) or ABHD12 knockout (−/−) mice following treatment with vehicle (DMSO) or lipopolysaccharide (LPS) or (*R*)-**2a–2h** (1 μM, 4 h, 37°C); All data are presented as mean ± SD (n = 4/group). *p < 0.05, **p < 0.01, ***p < 0.001 versus (+/+) group by Student's two-tailed unpaired parametric t test.

Cellular carboxylesterases metabolize Me-lyso-PS to lyso-PS

Having synthesized Me-lyso-PSs, we postulated that these might be metabolized by cellular carboxylesterases to yield the corresponding lyso-PSs (Figure 2A). To test this hypothesis, we incubated three (*R*)-Me-lyso-PSs of varying lipid tails ((*R*)-**2b** [C12:0, medium-chain], (*R*)-**2e** [C18:0, LC], or (*R*)-**2b** [C24:0, VLC]) with active or denatured porcine liver carboxylesterase, and upon this treatment, by LC-MS (Joshi et al., 2018) we checked for the formation of the corresponding canonical lyso-PSs. We found for all the three (*R*)-Me-lyso-PSs subjected to this treatment that upon incubation with active but not the denatured carboxylesterase, the (*R*)-Me-lyso-PS was completely consumed and a new peak was observed with mass shift of ∼14 Da (parent *m/z* − 14 Da) (Figure 2A). The mass of this new peak corresponds to the loss of the methyl group from (*R*)-Me-lyso-PS to yield the corresponding canonical (*R*)-lyso-PS via hydrolysis by the carboxylesterase (Figure 2A). Since we planned to test this synthetic Me-lyso-PS library for different biological activities in mammalian macrophages and mast cells, we decided to test whether lysates of these immune cells had carboxylesterases capable of converting (*R*)-Me-lyso-PSs to the canonical lyso-PSs. To negate any lyso-PS lipase type activity, we used active or denatured lysates from ABHD12-null primary peritoneal macrophages or peritoneal-derived cultured mast cells, and found that the active but not denatured lysates from both these immune cells converted the three previously tested (*R*)-Me-lyso-PSs, namely, (*R*)-**2b** (C12:0, medium-chain), (*R*)-**2e** (C18:0, LC), and (*R*)-**2h** (C24:0, VLC), to their corresponding canonical (*R*)-lyso-PS lipid (Figure S2A). Our results clearly show that cellular carboxylesterases can hydrolyze the methyl group of (*R*)-Me-lyso-PSs to yield the corresponding canonical (*R*)-lyso-PSs (Figure 2A) and that the synthetic Me-lyso-PSs serve as stable prodrug-like biological surrogates to lyso-PSs, making them amenable to testing in primary macrophages and mast cells.

VLC lyso-PSs elicit robust pro-inflammatory responses in mammalian macrophages

Lyso-PSs have previously been shown to elicit immunological responses via pro-inflammatory cytokine secretion (e.g., tumor necrosis factor α [TNF-α], interleukin-6 [IL-6]) from mammalian macrophages (Kamat et al., 2015; Frasch and Bratton, 2012), and we wanted to assess whether the Me-lyso-PSs were capable of the same, having shown that carboxylesterases in primary macrophages can metabolize Me-lyso-PSs to lyso-PSs (Figure S2A). We found that when primary peritoneal macrophages (PPMs) isolated from wild-type (WT) mice were treated with equal concentrations of the canonical LC lyso-PSs (**1a** [C16:0] and **1b** [C18:0]) and the corresponding (*R*)-Me-lyso-PSs ((*R*)-**2d** and (*R*)-**2e**) of the same lipid tail, they secreted almost equal amounts of pro-inflammatory cytokines (TNF-α, IL-6) (Figure S2B). Not surprisingly, treating PPMs with unnatural (*S*)-Me-lyso-PSs (Figure S2C), corresponding free fatty acids (Figure S2C), or other lysophospholipids (lysophosphatidic acid [lyso-PA], lysophosphatidylglycerol [lyso-PG], and lysophosphatidylcholine [lyso-PC]) with same lipid tail (Figure S2D) failed to elicit any inflammatory response, suggesting that ligand recognition in PPMs in eliciting pro-inflammatory responses is highly stereospecific for (*R*)-lyso-PSs. Having established comparable bioactivities of canonical lyso-PSs and (*R*)-Me-lyso-PSs, we isolated PPMs from WT or ABHD12

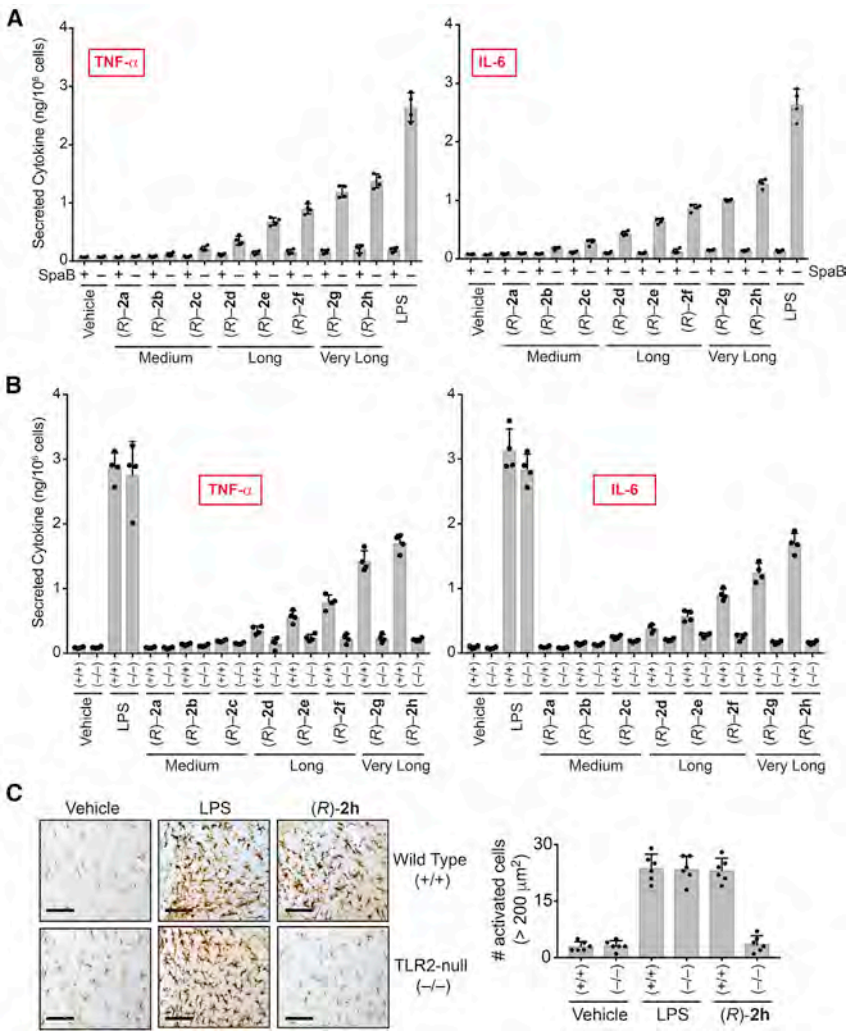

Figure 3. VLC lyso-PSs elicit pro-inflammatory responses via a TLR2-dependent pathway

(A and B) Secreted TNF-α and IL-6 from PPMs harvested from: (A) WT mice pre-treated with DMSO or SpaB (10 μM, 4 h, 37°C), followed by treatment with vehicle or LPS or (*R*)-**2a–2h** (1 μM, 4 h, 37°C); (B) WT (+/+) or TLR2 knockout (–/–) mice following treatment with vehicle or LPS or (*R*)-**2a–2h** (1 μM, 4 h, 37°C).

(C) Representative images from Iba-1 immunostaining for microglial activation (scale bars, 250 μm) and quantification of enlarged cells (>200 μm^2) in the cerebellum (per 1.44 mm^2) of WT (+/+) or TLR2 knockout (–/–) mice following intravenous injection of vehicle (PBS), LPS, or (*R*)-**2h** (C24:0) (all 1 mg/kg body weight, 10 h).

All data are presented as mean ± SD (n = 4–6/group).

knockout mice and incubated them with the (*R*)-Me-lyso-PS library to determine whether the length of lipid tail had any effect on pro-inflammatory cytokine secretion. Interestingly, we found from this SAR study that VLC (*R*)-Me-lyso-PSs, particularly (*R*)-**2g** (C22:0) and (*R*)-**2h** (C24:0), produced the highest pro-inflammatory cytokine secretion (TNF-α, IL-6) from WT PPMs (Figure 2B). Not surprisingly, ABHD12-null PPMs secreted significantly more pro-inflammatory cytokines compared with WT PPMs upon (*R*)-Me-lyso-PS treatments, consistent with their diminished lyso-PS lipase activity (Kamat et al., 2015) (Figure 2B). For either genotype, the pharmacological Me-lyso-PS treatments did not have any effect on cell viability.

Here, we used the bacterial outer membrane glycolipid lipopolysaccharide (LPS) as a positive control, as this endotoxin tested in PPMs mimics Gram-negative bacteria and robustly elicits immunological responses (pro-inflammatory cytokine secretion) in PPMs toward clearing this infection via a TLR4-dependent pathway (Raetz and Whitfield, 2002). In these assays, we found that the VLC (*R*)-Me-lyso-PS treatments produced ~60% pro-inflammatory cytokine secretion relative to similar LPS treatments in PPMs, suggesting that like LPS, VLC (*R*)-Me-lyso-PSs are potent immunological activators in mammalian macrophages (Figure 2B). We also performed a similar SAR study in human THP-1 macrophages and found similar results whereby VLC (*R*)-Me-lyso-PSs produced the highest secretion of pro-inflammatory cytokines (Figure S2E).

VLC lyso-PSs signal via TLR2 in mammalian macrophages

Reported literature speculates that VLC lyso-PSs perhaps signal through TLR2 (Van Der Kleij et al., 2002) although, to the best of our knowledge, VLC lyso-PSs have never been directly tested against any receptor for any immunological activity given their commercial unavailability. We found from a large-scale gene expression database (Figure S3A) (Wu et al., 2016) and by RT-PCR analysis (Figure S3B) that TLR2 (but none of the other putative lyso-PS receptors [Inoue et al., 2012]) is enriched on WT PPMs. Next, we found that pharmacological antagonism of TLR2 using Sparstolonin B (SpaB) (Liang et al., 2011) ablated the increased pro-inflammatory cytokine secretion caused by VLC (*R*)-Me-lyso-PS treatments in WT PPMs (Figure 3A), and in human THP-1 macrophages (Figure S2F). Here, we found that SpaB treatment also ablated the increased pro-inflammatory cytokine secretion caused by LPS treatment in WT PPMs (Figure 3A), consistent with SpaB's dual TLR2/TLR4 antagonism activity (Liang et al., 2011, 2013). Furthermore, we harvested PPMs from TLR2 knockout mice (Figure S3C) (Holla et al., 2016) and measured pro-inflammatory cytokine secretion following (*R*)-Me-lyso-PS treatments. Consistent with the pharmacological studies, we found that VLC (*R*)-Me-lyso-PSs, particularly (*R*)-**2g** and (*R*)-**2h**, produced highest secretion of TNF-α and IL-6 from WT PPMs, and this pro-inflammatory cytokine secretion was almost absent in TLR2-null PPMs (Figure 3B).

ABHD12 knockout mice display increased cerebellar microgliosis, whereby the accumulation of VLC lyso-PSs speculatively causes this neuroinflammatory phenotype (Blankman et al., 2013). To test whether VLC lyso-PSs indeed causes

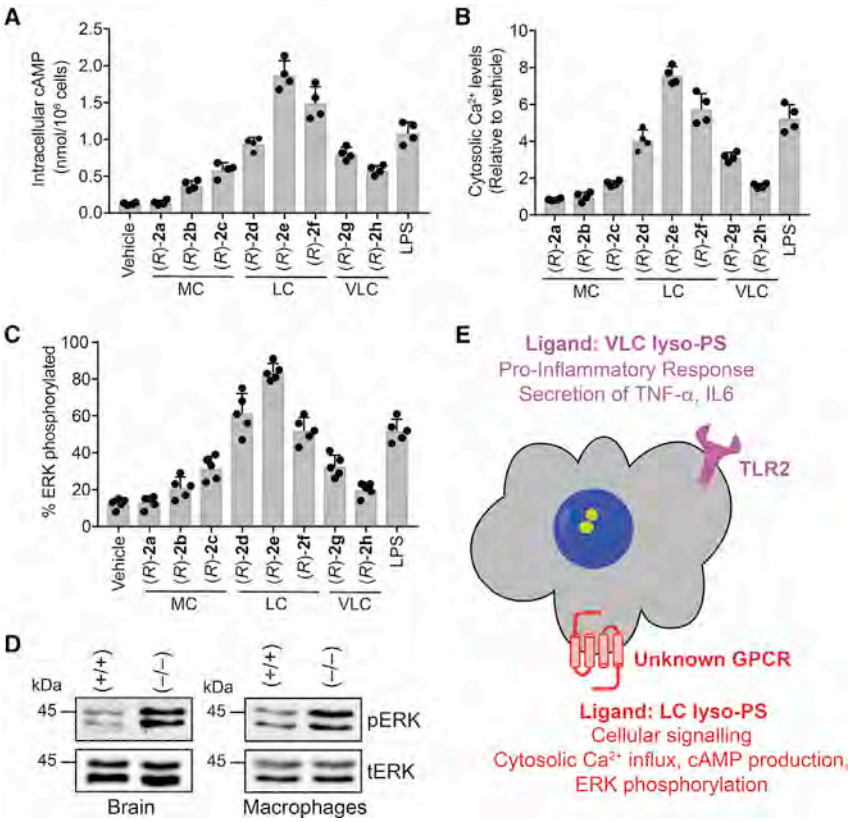

Figure 4. LC lyso-PSs activate macrophages through a putative GPCR

(A–C) (A) Intracellular cAMP, (B) relative cytosolic Ca^{2+} levels, and (C) percentage of phosphorylated ERK from WT PPMs following treatment with vehicle (DMSO) or LPS or (*R*)-**2a–2h** (1 μM, 10 min, 37°C). All data are presented as mean ± SD (n = 4–5/group), where MC denotes medium chain, LC long chain, and VLC very long chain.

(D) Representative western blots on lysates from brains (6-month-old mice) and LPS-treated (1 μM, 4 h, 37°C) PPMs harvested from WT (+/+) or ABHD12-null (−/−) mice, showing enhanced phosphorylation of ERK in both these tissues for the ABHD12-null (−/−) genotype.

(E) Schematic representation summarizing the lyso-PS signaling pathways by possibly two types of receptors on mammalian macrophages.

neuroinflammation and if they signal through TLR2, we intravenously injected a VLC (*R*)-Me-lyso-PS ((*R*)-**2h**, C24:0) into WT or TLR2-null mice, and quantified the extent of neuroinflammation by counting the number of activated microglia using an established immunohistochemical protocol (Singh et al., 2020; Blankman et al., 2013). We found that systemic administration of (*R*)-**2h** (C24:0) robustly induced cerebellar microgliosis in WT but not TLR2 knockout mice, suggesting that VLC (*R*)-Me-lyso-PSs signals through TLR2, causing neuroinflammation (Figures 3C and S4). As a positive control, we used LPS (which signals through TLR4) (Raetz and Whitfield, 2002) and intravenously injected it at the same dose and time, and found that the extent of neuroinflammation in WT and TLR2-null mice was almost identical (Figures 3C and S4). Furthermore, we found that relative to the positive control LPS, the VLC (*R*)-Me-lyso-PS (*R*)-**2h** (C24:0) produced comparable neuroinflammation (Figures 3C and S4). Interestingly, a LC (*R*)-Me-lyso-PS ((*R*)-**2e**, C18:0) intravenous injection for the same dosing regimen did not produce any neuroinflammation in WT mice (Figures S4A and S4B). Taken together, our results provide compelling *in vivo* evidence that VLC lyso-PSs (but not LC lyso-PSs) signal through TLR2, elicit a robust pro-inflammatory immune response, and are likely responsible for the neuroinflammation observed in ageing ABHD12 knockout mice, the murine model of PHARC (Blankman et al., 2013).

Mammalian macrophages have a cryptic lyso-PS receptor

Mammalian macrophages in response to lyso-PS produce increased intracellular cyclic adenosine 5′-monophosphate (cAMP) (Sugita et al., 2013), cytosolic calcium (Ca^{2+}) influx (Park et al., 2005), and heightened phosphorylation of the nodal extracellular signal-regulated kinase (ERK) (Lee et al., 2008; Sugita et al., 2013), and we wanted to test whether Me-lyso-PSs also produce these phenotypes in mammalian macrophages. We found in WT PPMs that cellular cAMP (Figure 4A), relative cytosolic Ca^{2+} levels (Figure 4B), and ERK phosphorylation (Figure 4C) increased most profoundly upon treatment with LC (*R*)-Me-lyso-PSs, especially (*R*)-**2e** (C18:0), and that medium-chain or VLC (*R*)-Me-lyso-PS had negligible effects on these phenotypes. Surprisingly, the genetic deletion of TLR2 in PPMs (Figures S5A, S5B, and S6C) or its pharmacological antagonism in PPMs (Figures S5C, S5D, and S6B) and human THP-1 macrophages (Figures S5E, S5F, and S6B) showed no change on any of these phenotypes following (*R*)-Me-lyso-PS treatment. We also found that the LC (*R*)-Me-lyso-PSs (*R*)-**2e** (C18:0) and the corresponding canonical lyso-PS **1b** (C18:0) behaved identically in all these assays (Figures S6D–S6F). Not surprisingly, upon treating PPMs with (*S*)-Me-lyso-PSs (Figures S6A, S6E, and S6F), the corresponding free fatty acids or other lysophospholipids with lipid tail (C18:0) (Figures S6D–S6F), failed to elicit any significant response in any of these assays under similar treatment conditions, suggesting that these phenotypes in mammalian macrophages are specific to LC (*R*)-Me-lyso-PS (particularly C18:0). In all these assays, we found that the pharmacological Me-lyso-PS treatments did not affect cell viability.

Of note, brains and LPS-treated PPMs derived from ABHD12-null mice (where, in absolute concentrations, **1b** [C18:0 lyso-PS] is the most abundant, and significantly deregulated lyso-PS [Blankman et al., 2013; Kamat et al., 2015]) have markedly more ERK phosphorylation compared with WT control (Figure 4D). Given the heightened intracellular cAMP, cytosolic Ca^{2+} influx, phosphorylation of ERK, and inability of pharmacological antagonism or genetic disruption of TLR2 to affect any of these phenotypes, strongly supports the existence of another cryptic lyso-PS receptor on mammalian macrophages (in

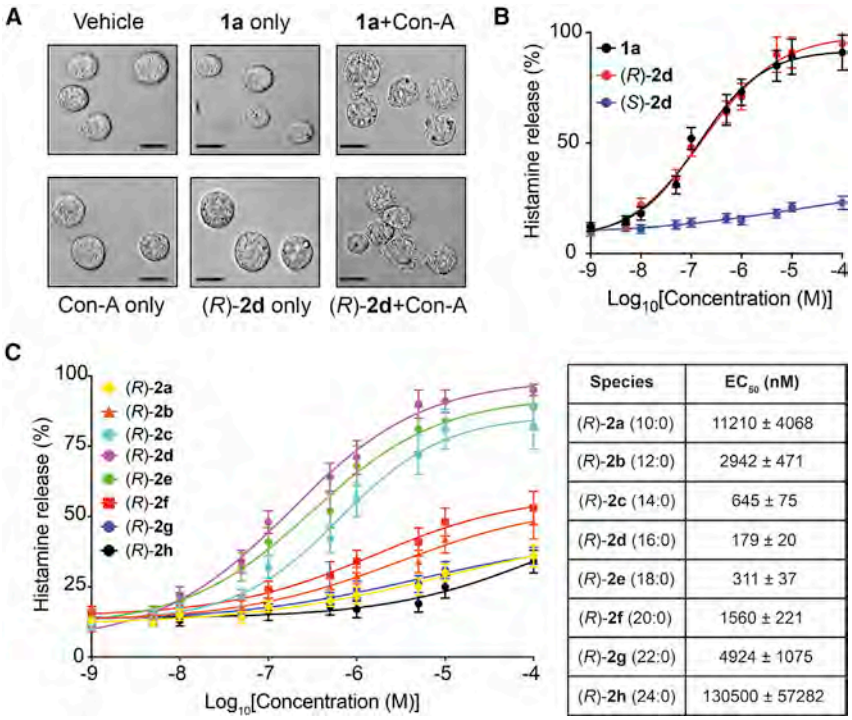

Species	EC_{50} (nM)
(*R*)-**2a** (10:0)	11210 ± 4068
(*R*)-**2b** (12:0)	2942 ± 471
(*R*)-**2c** (14:0)	645 ± 75
(*R*)-**2d** (16:0)	179 ± 20
(*R*)-**2e** (18:0)	311 ± 37
(*R*)-**2f** (20:0)	1560 ± 221
(*R*)-**2g** (22:0)	4924 ± 1075
(*R*)-**2h** (24:0)	130500 ± 57282

Figure 5. LC lyso-PSs robustly cause histamine release from primary mast cells

(A) Representative microscopy image showing degranulation of PCMCs after **1a** (C16:0 lyso-PS) or (*R*)-**2d** (C16:0) treatment (both 1 μM, 30 min, 37°C) in the presence of concanavalin A (Con-A). Scale bars, 100 μm.

(B) Histamine release profile from PCMCs treated with **1a** (C16:0 lyso-PS), (*R*)-**2d** (C16:0), or (*S*)-**2d** (C16:0) (1 nM to 10 mM, 30 min, 37°C, n = 3/data point).

(C) Dose-response and EC_{50} values for histamine release from PCMCs following treatment with the different (*R*)-Me-lyso-PSs (1 nM to 10 mM, 30 min, 37°C, n = 3/data point).

addition to TLR2) (Figure 4E). We speculate, based on aforementioned phenotypes, that this as yet unknown receptor is likely an unannotated GPCR (as putative lyso-PS GPCRs [Inoue et al., 2012] are absent in macrophages [Figures S3A and S3B]) that prefers LC lyso-PSs (particularly C18:0) as ligands to produce its downstream biological effects (Figure 4E).

LC lyso-PSs robustly induce mast cell degranulation

The release of histamine during mast cell degranulation is an extensively investigated lyso-PS-mediated immunological response (Sugo et al., 2006; Iwashita et al., 2009; Shanbhag et al., 2020), and yet contribution of individual lyso-PSs to this phenotype remain poorly understood. To address this, we generated peritoneal-derived cultured mast cells (PCMCs) (Meurer et al., 2016), and confirmed their ability to degranulate in the presence of **1a** (C16:0 lyso-PS) or the corresponding (*R*)-Me-lyso-PS, (*R*)-**2d** (C16:0) in the presence of concanavalin A (Con-A) (Figure 5A) (Iwashita et al., 2009; Sugo et al., 2006). Con-A is a well-characterized metalloprotein lectin of interest to immunologists, as it specifically binds mannosyl and/or glucosyl units of surface receptors of immune cells, and in doing so stabilizes receptor conformations that, in the context of PCMCs, facilitate lyso-PS-dependent histamine release (Lawson et al., 1978; Sullivan et al., 1975). Having shown their ability to degranulate, we quantitatively measured the histamine release from PCMCs using an established LC-MS method (Chimalakonda et al., 2015) (Figure S7). We found that the half-maximal effective concentration (EC_{50}) toward inducing histamine release during degranulation in PCMCs for **1a** (C16:0 lyso-PS, EC_{50} = 140 ± 22 nM) and (*R*)-**2d** (C16:0, EC_{50} = 179 ± 20 nM) were comparable, while the unnatural (*S*)-**2d** (C16:0, EC_{50} > 10 μM) failed to produce this phenotype (Figure 5B), suggesting that the putative receptor on PCMCs (likely GPR34 [Iwashita et al., 2009; Sugo et al., 2006; Ikubo et al., 2015], Figure S3A) is stereoselective in lyso-PS recognition. Next, we performed exhaustive dose-response studies with the (*R*)-Me-lyso-PS library and found that (*R*)-**2d** (C16:0, EC_{50} = 179 ± 20 nM) most potently induced histamine release during PCMC degranulation, with other LC (*R*)-Me-lyso-PSs (*R*)-**2e** (C18:0, EC_{50} = 311 ± 37 nM) and (*R*)-**2c** (C14:0, EC_{50} = 645 ± 75 nM) following suit (Figure 5C). This SAR study showed that medium-chain (<C12) or VLC (≥C20) (*R*)-Me-lyso-PSs failed to induce significant PCMC degranulation (EC_{50} > 2.5 μM) (Figure 5C), suggesting that besides the headgroup, the recognition of lipid tail is another major factor contributing to histamine release from mast cells during degranulation. In this SAR study, we found that the pharmacological Me-lyso-PS treatments had no effect on cell viability.

ABHD12 is the major lyso-PS lipase in primary mast cells

ABHD12 is a major lyso-PS lipase in different immune cells (Ogasawara et al., 2018; Kamat et al., 2015), but its biochemical function in primary mast cells remains unknown. Western blot analysis (Figure 6A) and diminished lyso-PS lipase activity (Figure 6B) confirmed the loss of ABHD12 in PCMCs derived from ABHD12-null mice. We also found that ABHD12-null PCMCs secreted significantly more lyso-PS (~2-fold more **1a** [C16:0] and **1b** [C18:0]) compared with WT PCMCs (Figure 6C). Given the diminished lyso-PS lipase activity, we postulated that **1a** (C16:0 lyso-PS) treatment would cause ABHD12-null PCMCs to degranulate at a lower dose of **1a**, and thereby release histamine more efficiently than WT PCMCs. Indeed, ABHD12-null PCMCs (EC_{50} = 47 ± 17 nM) released histamine more effectively than WT PCMCs (EC_{50} = 135 ± 32 nM) upon similar **1a** (C16:0 lyso-PS) treatment (Figure 6D). Finally, we measured serum histamine concentrations following intravenous (*R*)-**2d** (C16:0) injection in WT or ABHD12 knockout mice and found that ABHD12-null mice displayed heightened circulating histamine concentrations (~3-fold) compared with WT mice (Figure 6E). These results together confirm ABHD12's role as a major lyso-PS lipase in primary mast cells, where by regulating serum lyso-PS levels (Figure 6E) it controls systemic histamine release (Figure 6E).

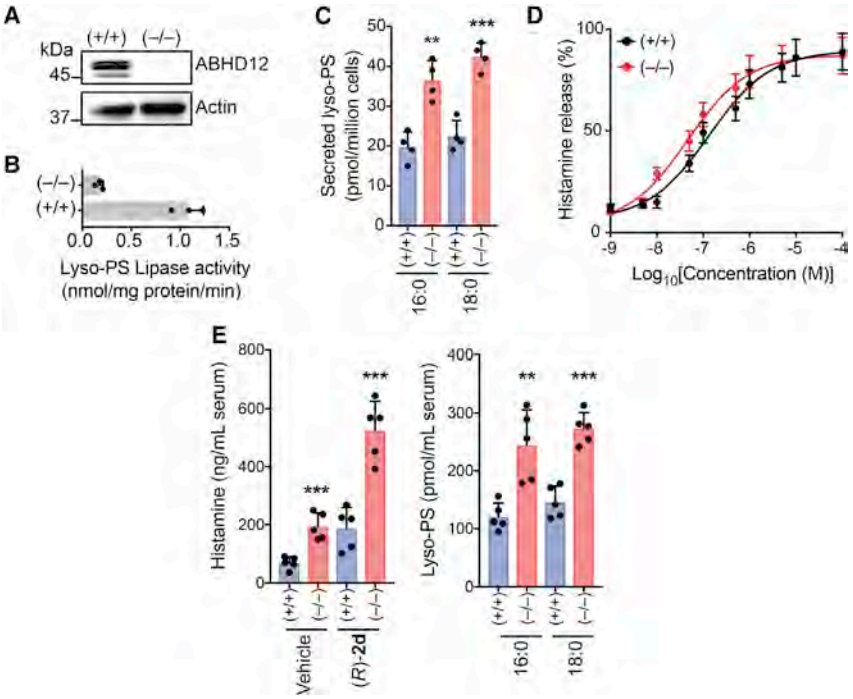

Figure 6. ABHD12 controls concentrations of LC lyso-PSs in primary mast cells, and thereby serum histamine levels

(A and B) (A) Representative western blot and (B) lyso-PS lipase activity assay (100 μM **1a** [C16:0 lyso-PS], 30 min, 37°C, n = 3/group), showing the loss of ABHD12 in PCMCs derived from ABHD12 knockout (−/−) mice.

(C) Concentrations of lyso-PS secreted from cultured PCMCs derived from WT (+/+) or ABHD12 knockout (−/−) mice, showing significantly increased **1a** (C16:0 lyso-PS) and **1b** (C18:0 lyso-PS) secretion from ABHD12-null PCMCs (n = 4/group).

(D) Histamine release profiles from PCMCs derived from WT (+/+) or ABHD12 knockout (−/−) mice treated with **1a** (C16:0 lyso-PS) (1 nM to 10 mM, 30 min, 37°C, n = 3/data point).

(E) Left: serum histamine levels in (+/+) or (−/−) mice following intravenous injections with vehicle (PBS) or (*R*)-**2d** (C16:0) (1 mg/kg, 2 h), showing increased serum histamine concentrations in the (−/−) mice compared with (+/+) controls for both treatments (n = 5/group). Interestingly, systemic administration of (*R*)-**2d** (C16:0) in (+/+) mice produces significantly more circulating serum histamine compared with the vehicle group, showing that (*R*)-**2d** (C16:0) by itself can induce histamine release from mast cells in *in vivo* settings. Right: serum lyso-PS concentrations in (+/+) or (−/−) mice, showing increased concentrations of circulating **1a** (C16:0 lyso-PS) and **1b** (C18:0 lyso-PS) in (−/−) mice, corroborating the increased serum histamine levels seen in these mice (n = 5/group). All data are presented as mean ± SD from at least n independent experiments. **p < 0.01, ***p < 0.001 versus (+/+) group by Student's two-tailed unpaired parametric t test.

DISCUSSION

Signaling lipids are potent hormone-like biological molecules that regulate several important physiological processes in mammals, and their deregulation often has detrimental consequences that eventually manifest as disease in humans. Given their direct link to human diseases, the lyso-PSs have been recently emerged as yet another important class of signaling lipids (Shanbhag et al., 2020). However, unlike the established signaling lipids (e.g., 2-AG, AEA, S1P), *in vivo* lyso-PSs exist esterified with different lipid tails ranging from medium-chain (C10–C14) to LC (C16–C20) to VLC (>C20) fatty acids (Kamat et al., 2015; Blankman et al., 2013; Singh et al., 2020). Given the vast diversity in their *in vivo* content, it remains unclear as to which of these lyso-PSs have signaling functions and how they influence, regulate, and/or modulate different immunological processes. The lack of detailed SAR studies for these immunological phenotypes for lyso-PSs stems largely from the limited commercial availability and reported synthetic strategies toward making them, especially the medium-chain and VLC variants.

In this paper, we report the synthesis of Me-lyso-PSs having (*R*)- or (*S*)-stereochemistry at the *sn*-2 position of the glycerol backbone with varying lipid tails ranging from medium-chain to LC to VLC (Figure 1 and Data S1). Since the synthesis of lyso-PSs has proved challenging, and that of VLC lyso-PSs has not been reported to the best of our knowledge, our synthetic strategy allows the performance of rigorous SAR studies in diverse assays to delineate the specific function of the lipid tail in modulating a phenotype regulated by lyso-PSs. In all our biochemical and immunological assays, we find that (*R*)-Me-lyso-PSs serve as excellent bioequivalent surrogates for the canonical (*R*)-lyso-PSs, while the corresponding (*S*)-Me-lyso-PSs are biologically inactive. Since VLC lyso-PSs have never been tested against ABHD12, despite their accumulation in the brains of ABHD12-null mice (Blankman et al., 2013; Singh et al., 2020), here, by assaying the Me-lyso-PS library, we show conclusively that the ABHD12-catalyzed lyso-PS lipase reaction is stereoselective and prefers VLC lyso-PSs as substrates (Figure 1). Furthermore, we show through biochemical assays that the (*R*)-Me-lyso-PSs are acted upon by cellular carboxylesterases and converted to the corresponding canonical (*R*)-lyso-PSs, and that therefore, biologically, the (*R*)-Me-lyso-PSs function as prodrug-like surrogates for lyso-PSs in primary macrophages and mast cells (Figure 2).

Next, we wanted to understand the distinct role played by the lipid tail of individual lyso-PSs in the activation of macrophages and mast cell degranulation, as these immunological processes have been extensively studied and reported to be regulated by lyso-PSs (Shanbhag et al., 2020). In mammalian macrophages, we find that VLC Me-lyso-PSs produce the highest secretion of pro-inflammatory cytokines and that these pro-inflammatory responses are higher in ABHD12-null macrophages (Figure 2), given their diminished lyso-PS lipase activity (Kamat et al., 2015). Next, using pharmacological tools and genetic models, we show conclusively that VLC Me-lyso-PSs (but not LC lyso-PSs) orchestrate robust pro-inflammatory responses via a TLR2-dependent pathway to cause neuroinflammation (Figure 3). That VLC lyso-PSs signal through TLR2 and cause neuroinflammation (Figures 3 and S4) raises an intriguing possibility, corroborating a recent report (Ogasawara et al., 2018) that the

human neurological disease PHARC may itself be an autoimmune disease. Furthermore, we find that mammalian macrophages produce increased intracellular cAMP, cytosolic Ca^{2+} flux, and heightened ERK phosphorylation in response to LC lyso-PS treatments (particularly C18:0 lyso-PS) (Figure 4) via a TLR2-independent pathway (Figures S5 and S6), and we speculate that there is another cryptic receptor, likely a GPCR, that prefers LC lyso-PSs (particularly C18:0 lyso-PS) as ligands to produce these biological activities (Figure 4). We also show that LC lyso-PSs (especially C16:0 lyso-PS), but not medium-chain or VLC lyso-PSs, efficiently cause the release of histamine from mast cells during degranulation, suggesting that the putative lyso-PS receptor on mast cells (possibly GPR34 [Sugo et al., 2006]) prefers LC lyso-PSs (particularly C16:0 lyso-PS) as ligands to drive this immunological process (Figure 5). Finally, we report that ABHD12 is the major lyso-PS lipase in primary mast cells, where it controls the secreted lyso-PS levels, and its deletion in mice results in elevated levels of serum histamine and lyso-PS (Figure 6).

Projecting ahead, we propose that the functional antagonism of TLR2 might provide an excellent therapeutic paradigm in treating PHARC. This premise can be tested genetically by generating and characterizing ABHD12-TLR2 dual-knockout mice, and pharmacologically by discovering much needed *in vivo* active TLR2 functional antagonists. In addition, the annotation of ABHD12 as a major lyso-PS lipase in primary mast cells provides yet another avenue in understanding the immunomodulatory properties and the functional crosstalk of lyso-PSs between different immune cells particularly in the context of allergies and autoimmune conditions (Kelkar et al., 2019; Ogasawara et al., 2018). Finally, we would like to note that a major shortcoming of our study is the inability of our synthetic strategy in making Me-lyso-PSs with unsaturated fatty acid chains. Therefore, the development of such a synthetic methodology would enable making Me-lyso-PSs with unsaturated fatty acid chains and could also be leveraged to generate lyso-PS probes with suitable recently reported biorthogonal handles (Niphakis et al., 2015). Such bifunctional lyso-PS probes in tandem with advanced MS-based chemoproteomics platforms (Niphakis et al., 2015; Parker et al., 2017) will greatly facilitate the identification of hitherto unknown lyso-PS protein ligands and/or receptors, and this emerging knowledge will certainly expand our biological understanding of this underexplored immunomodulatory lipid class.

SIGNIFICANCE

Lysophospholipids are potent hormone-like biological mediators that regulate many important physiological processes in mammals. Recently, the lysophosphatidylserines (lyso-PSs) have emerged as yet another class of signaling lysophospholipids, with potent bioactivities in the central nervous and immune system in mammals, and deregulation in their metabolism has been linked to neurological and autoimmune disorders in humans. However, challenges in making lyso-PSs synthetically, and limited commercial sources for this lipid class, have greatly hampered any exhaustive structure-activity relationship (SAR) studies toward mechanistically understanding the role that lyso-PSs play in different physiological processes. Here, we report a synthetic strategy toward making methyl esters of lyso-PSs (Me-lyso-PSs) with varying lipid tails, which serve as excellent prodrug-like biological surrogates for lyso-PSs, and focus on elucidating the role that the lipid tail of this lysophospholipid plays in regulating various immunological processes. Specifically, we study the lyso-PS-mediated activation of macrophages and mast cell degranulation processes, and show through detailed SAR studies that the lipid tail has profound effects on the phenotypical outputs of these important immunological processes. Our findings thus illuminate a physiological balance between long-chain and very-long-chain lyso-PSs, intricately regulated by the lyso-PS lipase ABHD12, and that disrupting this fine-tuned homeostasis results in immunological outputs that have detrimental pathological consequences in humans.

STAR★METHODS

Detailed methods are provided in the online version of this paper and include the following:

- KEY RESOURCES TABLE
- RESOURCE AVAILABILITY
  - Lead contact
  - Materials availability
  - Data and code availability
- EXPERIMENTAL MODEL AND SUBJECT DETAILS
  - Mice
  - Mammalian cell lines
- METHOD DETAILS
  - Reagents
  - Lyso-PS lipase substrate assays
  - Mammalian cells lipid treatments
  - Western blot analysis
  - ELISA assays
  - RT-PCR
  - Immunohistochemical analysis
  - Histamine estimation from mast cells
  - Lyso-PS measurements
  - Synthesis and compound characterization
- QUANTIFICATION AND STATISTICAL ANALYSIS

SUPPLEMENTAL INFORMATION

Supplemental information can be found online at https://doi.org/10.1016/j.chembiol.2021.01.008.

ACKNOWLEDGMENTS

This work was supported by a DBT/Wellcome Trust India Alliance Fellowship (grant number IA/I/15/2/502058) awarded to S.S.K., a Department of Science and Technology (DST) Fund for Improvement of S&T Infrastructure (grant number SR/FST/LSII-043/2016) to the IISER Pune Biology Department, and a J.C. Bose National Fellowship from the Science & Engineering Research Board (SERB) (grant number SB/S2/JCB-025/2016) awarded to K.N.B. N.K. acknowledges a SERB postdoctoral fellowship, and M.S. acknowledges a graduate student fellowship from the Council of Scientific and Industrial Research. Benjamin F. Cravatt of The Scripps Research Institute is thanked for providing the ABHD12 knockout mice used in this study. The National Facility for Gene Function in Health and Disease (NFGFHD) at IISER Pune (supported by a grant from the Department of Biotechnology, Govt. of India; BT/INF/22/SP17358/2016) and

Central Animal Facility at IISc Bangalore are thanked for maintaining and providing mice for this study. Sagar Tarate and Dhanashree Kelkar are thanked for technical assistance. Vineeta Bal, Satyajit Rath, Girish Deshpande, Girish Ratnaparkhi, and Nishad Matange are thanked for reading and providing critical inputs to the manuscript.

AUTHOR CONTRIBUTIONS

N.K., S.S., T.S., and A.J. performed all the biochemical studies. M.S. and A.M. synthesized and characterized all the compounds; A.M. and H.C. supervised the synthesis. K.N.B. provided the TLR2 knockout mice for this study. S.S.K. conceived the project, acquired funding, analyzed the data and wrote the paper with input from all authors.

DECLARATION OF INTERESTS

The authors declare no competing interests.

Received: August 31, 2020
Revised: November 30, 2020
Accepted: January 6, 2021
Published: February 10, 2021

REFERENCES

Barnes, M.J., Li, C.M., Xu, Y., An, J., Huang, Y., and Cyster, J.G. (2015). The lysophosphatidylserine receptor GPR174 constrains regulatory T cell development and function. J. Exp. Med. *212*, 1011–1020.

Benjamini, Y., Krieger, A.M., and Yekutieli, D. (2006). Adaptive linear step-up procedures that control the false discovery rate. Biometrika *93*, 491–507.

Blankman, J.L., and Cravatt, B.F. (2013). Chemical probes of endocannabinoid metabolism. Pharmacol. Rev. *65*, 849–871.

Blankman, J.L., Long, J.Z., Trauger, S.A., Siuzdak, G., and Cravatt, B.F. (2013). ABHD12 controls brain lysophosphatidylserine pathways that are deregulated in a murine model of the neurodegenerative disease PHARC. Proc. Natl. Acad. Sci. U S A *110*, 1500–1505.

Blankman, J.L., Simon, G.M., and Cravatt, B.F. (2007). A comprehensive profile of brain enzymes that hydrolyze the endocannabinoid 2-arachidonoylglycerol. Chem. Biol. *14*, 1347–1356.

Chimalakonda, K.C., Pang, E., Weaver, J.L., Howard, K.E., Patel, V., and Boyne, M.T. (2015). Development and validation of a liquid-chromatography tandem mass spectrometry method to determine in vitro and in vivo histamine release. J. Pharm. Biomed. Anal. *102*, 494–499.

Chu, X., Shen, M., Xie, F., Miao, X.J., Shou, W.H., Liu, L., Yang, P.P., Bai, Y.N., Zhang, K.Y., Yang, L., et al. (2013). An X chromosome-wide association analysis identifies variants in GPR174 as a risk factor for Graves' disease. J. Med. Genet. *50*, 479–485.

Contos, J.J.A., Ishii, I., and Chun, J. (2000). Lysophosphatidic acid receptors. Mol. Pharm. *58*, 1188–1196.

Dennis, E.A. (2016). Lipidomics in disease and drug discovery. Faseb J. *30*, https://doi.org/10.1096/fasebj.30.1_supplement.114.3.

Dennis, E.A., and Norris, P.C. (2015). Eicosanoid storm in infection and inflammation. Nat. Rev. Immunol. *15*, 511–523.

Fahy, E., Cotter, D., Sud, M., and Subramaniam, S. (2011). Lipid classification, structures and tools. Biochim. Biophys. Acta *1811*, 637–647.

Fahy, E., Subramaniam, S., Brown, H.A., Glass, C.K., Merrill, A.H., Jr., Murphy, R.C., Raetz, C.R., Russell, D.W., Seyama, Y., Shaw, W., et al. (2005). A comprehensive classification system for lipids. J. Lipid Res. *46*, 839–861.

Fiskerstrand, T., H'mida-Ben Brahim, D., Johansson, S., M'zahem, A., Haukanes, B.I., Drouot, N., Zimmermann, J., Cole, A.J., Vedeler, C., Bredrup, C., et al. (2010). Mutations in ABHD12 cause the neurodegenerative disease PHARC: an inborn error of endocannabinoid metabolism. Am. J. Hum. Genet. *87*, 410–417.

Fiskerstrand, T., Knappskog, P., Majewski, J., Wanders, R.J., Boman, H., and Bindoff, L.A. (2009). A novel Refsum-like disorder that maps to chromosome 20. Neurology *72*, 20–27.

Fowler, C.J., Holt, S., Nilsson, O., Jonsson, K.O., Tiger, G., and Jacobsson, S.O. (2005). The endocannabinoid signaling system: pharmacological and therapeutic aspects. Pharmacol. Biochem. Behav. *81*, 248–262.

Frasch, S.C., and Bratton, D.L. (2012). Emerging roles for lysophosphatidylserine in resolution of inflammation. Prog. Lipid Res. *51*, 199–207.

Gardell, S.E., Dubin, A.E., and Chun, J. (2006). Emerging medicinal roles for lysophospholipid signaling. Trends Mol. Med. *12*, 65–75.

Gonzalez-Cabrera, P.J., Brown, S., Studer, S.M., and Rosen, H. (2014). S1P signaling: new therapies and opportunities. F1000prime Rep. *6*, 109.

Holla, S., Prakhar, P., Singh, V., Karnam, A., Mukherjee, T., Mahadik, K., Parikh, P., Singh, A., Rajmani, R.S., Ramachandra, S.G., and Balaji, K.N. (2016). MUSASHI-mediated expression of JMJD3, a H3K27me3 demethylase, is involved in foamy macrophage generation during mycobacterial infection. PLoS Pathog. *12*, e1005814.

Hosono, H., Aoki, J., Nagai, Y., Bandoh, K., Ishida, M., Taguchi, R., Arai, H., and Inoue, K. (2001). Phosphatidylserine-specific phospholipase A1 stimulates histamine release from rat peritoneal mast cells through production of 2-acyl-1-lysophosphatidylserine. J. Biol. Chem. *276*, 29664–29670.

Ikubo, M., Inoue, A., Nakamura, S., Jung, S.J., Sayama, M., Otani, Y., Uwamizu, A., Suzuki, K., Kishi, T., Shuto, A., et al. (2015). Structure-activity relationships of lysophosphatidylserine analogs as agonists of G-protein-coupled receptors GPR34, P2Y10, and GPR174. J. Med. Chem. *58*, 4204–4219.

Inoue, A., Ishiguro, J., Kitamura, H., Arima, N., Okutani, M., Shuto, A., Higashiyama, S., Ohwada, T., Arai, H., Makide, K., and Aoki, J. (2012). TGFalpha shedding assay: an accurate and versatile method for detecting GPCR activation. Nat. Methods *9*, 1021–1029.

Ishii, I., Fukushima, N., Ye, X., and Chun, J. (2004). Lysophospholipid receptors: signaling and biology. Annu. Rev. Biochem. *73*, 321–354.

Iwashita, M., Makide, K., Nonomura, T., Misumi, Y., Otani, Y., Ishida, M., Taguchi, R., Tsujimoto, M., Aoki, J., Arai, H., and Ohwada, T. (2009). Synthesis and evaluation of lysophosphatidylserine analogues as inducers of mast cell degranulation. Potent activities of lysophosphatidylthreonine and its 2-deoxy derivative. J. Med. Chem. *52*, 5837–5863.

Joshi, A., Shaikh, M., Singh, S., Rajendran, A., Mhetre, A., and Kamat, S.S. (2018). Biochemical characterization of the PHARC-associated serine hydrolase ABHD12 reveals its preference for very-long-chain lipids. J. Biol. Chem. *293*, 16953–16963.

Kamat, S.S., Camara, K., Parsons, W.H., Chen, D.H., Dix, M.M., Bird, T.D., Howell, A.R., and Cravatt, B.F. (2015). Immunomodulatory lysophosphatidylserines are regulated by ABHD16A and ABHD12 interplay. Nat. Chem. Biol. *11*, 164–171.

Kelkar, D.S., Ravikumar, G., Mehendale, N., Singh, S., Joshi, A., Sharma, A.K., Mhetre, A., Rajendran, A., Chakrapani, H., and Kamat, S.S. (2019). A chemical-genetic screen identifies ABHD12 as an oxidized-phosphatidylserine lipase. Nat. Chem. Biol. *15*, 169–178.

Kimura, I., Moritani, Y., and Tanizaki, Y. (1973). Basophils in bronchial asthma with reference to reagin-type allergy. Clin. Allergy *3*, 195–202.

Lawson, D., Fewtrell, C., and Raff, M.C. (1978). Localized mast cell degranulation induced by concanavalin A-Sepharose beads. Implications for the Ca2+ hypothesis of stimulus-secretion coupling. J. Cell Biol. *79*, 394–400.

Lee, S.Y., Lee, H.Y., Kim, S.D., Jo, S.H., Shim, J.W., Lee, H.J., Yun, J., and Bae, Y.S. (2008). Lysophosphatidylserine stimulates chemotactic migration in U87 human glioma cells. Biochem. Biophys. Res. Commun. *374*, 147–151.

Liang, Q.L., Wu, Q.A., Jiang, J.H., Duan, J.A., Wang, C., Smith, M.D., Lu, H., Wang, Q., Nagarkatti, P., and Fan, D.P. (2011). Characterization of Sparstolonin B, a Chinese herb-derived compound, as a selective toll-like receptor antagonist with potent anti-inflammatory properties. J. Biol. Chem. *286*, 26470–26479.

Liang, Q.L., Yu, F., Cui, X.D., Duan, J.A., Wu, Q.N., Nagarkatti, P., and Fan, D.P. (2013). Sparstolonin B suppresses lipopolysaccharide-induced inflammation in human umbilical vein endothelial cells. Arch. Pharmacal Res. *36*, 890–896.

Lloret, S., and Moreno, J.J. (1995). Ca^{2+} influx, phosphoinositide hydrolysis, and histamine release induced by lysophosphatidylserine in mast cells. J. Cell Physiol. *165*, 89–95.

Mallik, S., Prasad, R., Bhattacharya, A., and Sen, P. (2018). Synthesis of phosphatidylserine and its stereoisomers: their role in activation of blood coagulation. ACS Med. Chem. Lett. *9*, 434–439.

Meurer, S.K., Ness, M., Weiskirchen, S., Kim, P., Tag, C.G., Kauffmann, M., Huber, M., and Weiskirchen, R. (2016). Isolation of mature (peritoneum-derived) mast cells and immature (bone marrow-derived) mast cell precursors from mice. PLoS One *11*, e0158104.

Napier, C., Mitchell, A.L., Gan, E., Wilson, I., and Pearce, S.H.S. (2015). Role of the X-linked gene GPR174 in autoimmune Addison's disease. J. Clin. Endocrinol. Metab. *100*, E187–E190.

Navia-Paldanius, D., Savinainen, J.R., and Laitinen, J.T. (2012). Biochemical and pharmacological characterization of human alpha/beta-hydrolase domain containing 6 (ABHD6) and 12 (ABHD12). J. Lipid Res. *53*, 2413–2424.

Niphakis, M.J., Lum, K.M., Cognetta, A.B., 3rd, Correia, B.E., Ichu, T.A., Olucha, J., Brown, S.J., Kundu, S., Piscitelli, F., Rosen, H., and Cravatt, B.F. (2015). A global map of lipid-binding proteins and their ligandability in cells. Cell *161*, 1668–1680.

Ogasawara, D., Ichu, T.A., Vartabedian, V.F., Benthuysen, J., Jing, H., Reed, A., Ulanovskaya, O.A., Hulce, J.J., Roberts, A., Brown, S., et al. (2018). Selective blockade of the lyso-PS lipase ABHD12 stimulates immune responses in vivo. Nat. Chem. Biol. *14*, 1099–1108.

Park, K.S., Lee, H.Y., Kim, M.K., Shin, E.H., and Bae, Y.S. (2005). Lysophosphatidylserine stimulates leukemic cells but not normal leukocytes. Biochem. Biophys. Res. Commun. *333*, 353–358.

Parker, C.G., Galmozzi, A., Wang, Y., Correia, B.E., Sasaki, K., Joslyn, C.M., Kim, A.S., Cavallaro, C.L., Lawrence, R.M., Johnson, S.R., et al. (2017). Ligand and target discovery by fragment-based screening in human cells. Cell *168*, 527–541 e29.

Pathak, D., Mehendale, N., Singh, S., Mallik, R., and Kamat, S.S. (2018). Lipidomics suggests a new role for ceramide synthase in phagocytosis. ACS Chem. Biol. *13*, 2280–2287.

Raetz, C.R., and Whitfield, C. (2002). Lipopolysaccharide endotoxins. Annu. Rev. Biochem. *71*, 635–700.

Rajendran, A., Vaidya, K., Mendoza, J., Bridwell-Rabb, J., and Kamat, S.S. (2020). Functional annotation of ABHD14B, an orphan serine hydrolase enzyme. Biochemistry *59*, 183–196.

Rosen, H., Stevens, R.C., Hanson, M., Roberts, E., and Oldstone, M.B. (2013). Sphingosine-1-phosphate and its receptors: structure, signaling, and influence. Annu. Rev. Biochem. *82*, 637–662.

Rueden, C.T., Schindelin, J., Hiner, M.C., Dezonia, B.E., Walter, A.E., Arena, E.T., and Eliceiri, K.W. (2017). ImageJ2: ImageJ for the next generation of scientific image data. BMC Bioinformatics *18*, 529.

Schindelin, J., Rueden, C.T., Hiner, M.C., and Eliceiri, K.W. (2015). The ImageJ ecosystem: an open platform for biomedical image analysis. Mol. Reprod. Dev. *82*, 518–529.

Shanbhag, K., Mhetre, A., Khandelwal, N., and Kamat, S.S. (2020). The lysophosphatidylserines—an emerging class of signalling lysophospholipids. J. Membr. Biol. *253*, 381–397.

Singh, S., Joshi, A., and Kamat, S.S. (2020). Mapping the neuroanatomy of ABHD16A, ABHD12, and lysophosphatidylserines provides new insights into the pathophysiology of the human neurological disorder PHARC. Biochemistry *59*, 2299–2311.

Sugita, K., Yamamura, C., Tabata, K., and Fujita, N. (2013). Expression of orphan G-protein coupled receptor GPR174 in CHO cells induced morphological changes and proliferation delay via increasing intracellular cAMP. Biochem. Biophys. Res. Commun. *430*, 190–195.

Sugo, T., Tachimoto, H., Chikatsu, T., Murakami, Y., Kikukawa, Y., Sato, S., Kikuchi, K., Nagi, T., Harada, M., Ogi, K., et al. (2006). Identification of a lysophosphatidylserine receptor on mast cells. Biochem. Biophys. Res. Commun. *341*, 1078–1087.

Sullivan, T.J., Greene, W.C., and Parker, C.W. (1975). Concanavalin A-induced histamine release from normal rat mast cells. J. Immunol. *115*, 278–282.

Szymanski, K., Miskiewicz, P., Pirko, K., Jurecka-Lubieniecka, B., Kula, D., Hasse-Lazar, K., Krajewski, P., Bednarczuk, T., and Ploski, R. (2014). rs3827440, a nonsynonymous single nucleotide polymorphism within GPR174 gene in X chromosome, is associated with Graves' disease in Polish Caucasian population. Tissue Antigens *83*, 41–44.

Tracey, T.J., Steyn, F.J., Wolvetang, E.J., and Ngo, S.T. (2018). Neuronal lipid metabolism: multiple pathways driving functional outcomes in health and disease. Front. Mol. Neurosci. *11*, 10.

Van Der Kleij, D., Latz, E., Brouwers, J.F., Kruize, Y.C., Schmitz, M., Kurt-Jones, E.A., Espevik, T., De Jong, E.C., Kapsenberg, M.L., Golenbock, D.T., et al. (2002). A novel host-parasite lipid cross-talk. Schistosomal lyso-phosphatidylserine activates toll-like receptor 2 and affects immune polarization. J. Biol. Chem. *277*, 48122–48129.

Vance, J.E. (2015). Phospholipid synthesis and transport in mammalian cells. Traffic *16*, 1–18.

Wu, C., Jin, X., Tsueng, G., Afrasiabi, C., and Su, A.I. (2016). BioGPS: building your own mash-up of gene annotations and expression profiles. Nucleic Acids Res. *44*, D313–D316.

Wymann, M.P., and Schneiter, R. (2008). Lipid signalling in disease. Nat. Rev. Mol. Cell Biol. *9*, 162–176.

Yanagida, K., and Valentine, W.J. (2020). Druggable lysophospholipid signaling pathways. Adv. Exp. Med. Biol. *1274*, 137–176.